AGU ADVANCING EARTH AND SPACE SCIENCES

Earth's Future

RESEARCH ARTICLE
10.1029/2024EF005822

Climate Change Likely to Intensify Storm-Driven Compound Flooding in an Exemplar UK Estuary

Charlotte Lyddon[1], Laura Devitt[2], Mirko Barada[3], Gemma Coxon[2], Jonathan Tinker[4], Thomas Coulthard[5], Andrew Barkwith[6], and Peter Robins[3]

[1]Department of Geography and Planning, University of Liverpool, Liverpool, UK, [2]School of Geographical Sciences, University of Bristol, Bristol, UK, [3]School of Ocean Sciences, Bangor University, Bangor, UK, [4]Met Office, Exeter, UK, [5]Department of Natural Sciences, Manchester Metropolitan University, Manchester, UK, [6]British Geological Survey, Nottingham, UK

Abstract Flood protection authorities are not prepared for compound flood risk in estuaries—now and in the face of climate change. Climate projections are rarely downscaled appropriately to assess future changes in storm surge and concurrent river discharge extremes, and their interactions to exacerbate flooding. This is the first time that hourly and fine spatial resolution (7/2.2 km sea level/precipitation), physically consistent, climate projections are used to assess changes in storm surge and river discharge-driven compound events. The analysis, applied to the Dyfi estuary, western UK, uses 12 downscaled perturbed parameter ensembles for the high-emissions "RCP8.5" scenario from a global climate model (HadGEM3-GC3.0). Residual surge and river discharge projections are assessed independently to identify changes in magnitudes and return periods—then combined to identify changing patterns of dependence and timing of compound events. Under RCP8.5 scenario to 2080, river discharge is expected to increase by 28%–29% for 1/20 and 1/50-year events. Extreme (95th percentile) discharge events are more likely to occur concurrently with extreme surges, and compound events will occur more often, and with a shorter time lag between peak surge and peak discharge—potentially compounding flooding further. The analysis provided forcing conditions representative of future 1 in 20-year and 1 in 50-year events used to simulate a potential increased flood footprint in the estuary. The research raises the question of the wider pattern of future compound events throughout the UK, and worldwide, highlighting the critical need for downscaled, coastal and fluvial projections to futureproof flood management strategies.

Plain Language Summary Effective flood protection strategies are essential as flooding remains one of the most devastating and costly challenges for communities worldwide, and the likelihood of extreme flood events is expected to increase due to climate change. Climate models rarely capture how storm surges and river floods interact to worsen flooding in estuarine environments. This study is the first time that state of the art climate projections are used to assess changes in the combined effect of extreme sea and river level in the Dyfi estuary, UK, under a high-emissions scenario (RCP8.5). By 2080, river floods could increase by 28%–29%, and extreme surges and river floods are likely to coincide more often, reducing the time between peak events. These findings highlight the urgent need for models to represent the processes that control coastal and estuarine flooding to support effective flood management globally.

Key Points:

- Novel physically consistent, hourly-resolution, hydrological and marine projections to assess future compound flood hazard
- Fluvial drivers of flooding are projected to exhibit greater changes in magnitude than storm-driven marine drivers
- Increased dependence and reduced time lag could amplify flood risk, meaning hazard assessments must include joint probability of drivers

Supporting Information:

Supporting Information may be found in the online version of this article.

Correspondence to:

C. Lyddon,
c.e.lyddon@liverpool.ac.uk

Citation:

Lyddon, C., Devitt, L., Barada, M., Coxon, G., Tinker, J., Coulthard, T., et al. (2025). Climate change likely to intensify storm-driven compound flooding in an exemplar UK estuary. *Earth's Future*, *13*, e2024EF005822. https://doi.org/10.1029/2024EF005822

Received 19 DEC 2024
Accepted 8 OCT 2025

Author Contributions:

Conceptualization: Charlotte Lyddon, Mirko Barada, Thomas Coulthard, Andrew Barkwith, Peter Robins
Data curation: Charlotte Lyddon, Laura Devitt, Mirko Barada, Gemma Coxon, Jonathan Tinker, Thomas Coulthard, Andrew Barkwith, Peter Robins
Formal analysis: Charlotte Lyddon, Mirko Barada, Peter Robins
Funding acquisition: Mirko Barada, Thomas Coulthard, Andrew Barkwith, Peter Robins
Investigation: Charlotte Lyddon, Mirko Barada, Thomas Coulthard, Andrew Barkwith, Peter Robins

1. Introduction

Communities throughout the world face urgent challenges from projected changes in natural hazards this century, and must develop, refine, and implement adaptation solutions as new understanding evolves (Toimil et al., 2020). This is especially pertinent in low-lying coastal areas. Globally, over 40% of the world's population live within 100 km of the coast (Reimann, 2023), with one billion people occupying land less than 10 m above current high tide limits, including 230 m below 1 m (Kulp & Strauss, 2019). 22 of the 32 largest cities in the world are located on estuaries (e.g., New York, Shanghai, London, Rio de Janeiro, Tokyo) and are vulnerable to co-dependant risks of sea-level rise (SLR) and coastal erosion, alongside risks associated with compound flooding (Lewis, Palmer, et al., 2019; Ward et al., 2018).

Compound flooding is a common coastal hazard, causing substantial damages and fatalities worldwide (Bevacqua et al., 2017; Wahl et al., 2015). Compound flooding can be a consequence of two mechanisms; first, extreme coastal water levels during an incoming tide can "hold" or even reverse river flows through the backwater effect (Hoitimk & Jay, 2016; Zhang et al., 2019). Second, severe storm events can generate storm surges through the

Methodology: Charlotte Lyddon, Laura Devitt, Mirko Barada, Gemma Coxon, Thomas Coulthard, Andrew Barkwith, Peter Robins
Project administration: Mirko Barada, Andrew Barkwith, Peter Robins
Resources: Charlotte Lyddon, Laura Devitt, Mirko Barada, Gemma Coxon, Jonathan Tinker, Thomas Coulthard, Andrew Barkwith, Peter Robins
Software: Charlotte Lyddon, Laura Devitt, Mirko Barada, Gemma Coxon, Jonathan Tinker, Thomas Coulthard, Peter Robins
Supervision: Charlotte Lyddon, Mirko Barada, Thomas Coulthard, Andrew Barkwith, Peter Robins
Validation: Charlotte Lyddon, Laura Devitt, Mirko Barada, Gemma Coxon, Jonathan Tinker, Thomas Coulthard, Peter Robins
Visualization: Charlotte Lyddon, Mirko Barada, Andrew Barkwith, Peter Robins
Writing – original draft: Charlotte Lyddon, Mirko Barada, Peter Robins
Writing – review & editing: Charlotte Lyddon, Laura Devitt, Mirko Barada, Gemma Coxon, Jonathan Tinker, Thomas Coulthard, Andrew Barkwith, Peter Robins

inverse barometer effect at the same time as heavy precipitation which increases runoff and river discharge (Hendry et al., 2019; Kew et al., 2013). The occurrence of high sea level and heavy precipitation at the same time or in close succession can amplify storm impacts for estuarine populations who sit at the interface of all flood drivers (Zscheischler & Seneviratne, 2017). Cyclone Nargis in Myanmar (Fritz et al., 2009), Hurricane Katrina in the US (Jonkman et al., 2009), Storm Desmond and Ciara in NW England (Ferranti et al., 2017), and Hurricane Harvey in the US (Emanuel, 2017), are examples of compound events that caused extensive damage and associated costs (Couasnon et al., 2020).

Climate change is already a driver of increasing flood hazard due to changes in sea level and precipitation conditions and increased natural variability (Kay et al., 2011, 2018; Malhi et al., 2020). Historic observations and reanalysis simulations of sea level, river discharge (Wang et al., 2024; Gudmundsson et al., 2021), and flood events show changing trends in the drivers of the occurrences of flooding, with nearly 40% of analyzed flood events linked to heavier precipitation (Alifu et al., 2022). Global analyses of tide gauge records reveal accelerated and sustained SLR over the 20th and 21st centuries, accompanied by an increase in extreme high-water events since 1970 (Haigh et al., 2014; Lowe et al., 2010; Meli et al., 2020, 2023; Menéndez & Woodworth, 2010; Pugh & Maul, 1999; Watson et al., 2015). However, challenges remain in separating out contributions to coastal flooding from mean sea level, storm surges, waves, and land movements (Howard et al., 2014, 2024). As such, compound flooding in estuaries is a growing threat due to accelerating SLR, variability in surge, and the intensification of river discharge associated with climate changes (Church et al., 2013; Hallegatte et al., 2013; Seneviratne et al., 2021; Yin et al., 2018).

Research has assessed estuarine flood hazards under climate change (Harrison et al., 2021) and focused on fluvial or coastal flood drivers individually (Bates et al., 2021; Wing et al., 2017). Hydrodynamic models parameterize uniform changes in flood drivers to show increased fluvial flood risk from intensified precipitation (Feyen et al., 2011; Kundzewicz & Pińskwar, 2022; Steinhausen et al., 2022) and greater coastal flood hazards driven by SLR (Neumann et al., 2015; Nicholls et al., 2021; Vitousek et al., 2017). Climate change will also likely influence the timing, magnitude, and interdependences between the drivers, measured by upper tail dependence (Ganguli et al., 2020; Zscheischler & Seneviratne, 2017). Therefore, assessments of the future dependence between storm surge and river discharge requires coherent projections of both drivers as their interplay underpins these complex flooding phenomena.

Global Climate Models (GCMs) generate estimates of future climate (IPCC, 2021; Seneviratne et al., 2021) following an inter-model agreement of climate scenarios, such as the Coupled Model Intercomparison Project (CMIP), used to inform change via Phase 5 (CMIP5) (Muis et al., 2020) and Phase 6 (CMIP6) (Chen et al., 2020; Li et al., 2021). *GCMs* from CMIP5 have been used in combination with hydrodynamic models to identify regional, future variability and trends in return periods across NW Europe, with probability of compound flooding increasing along parts of northern Europe (Bevacqua et al., 2019). However, the coarse spatial resolution of GCMs (~1–3°) can introduce biases and uncertainty in the representation of the drivers of compound floods at estuary-scales (Maraun et al., 2015; Schaller et al., 2020)—in particular, underestimating extremes (Marsooli et al., 2019; Muis et al., 2016). Key physical processes are not included in GCMs, for example, shelf seas are under-represented in GCMs due to the absence of tides (Hermans et al., 2020; Tinker et al., 2020).

The UK Climate Projections (UKCP18) use the HadGEM3-GC3.05 GCM, with 12 perturbed parameter ensemble members (UKCP18 GCM–PPE) to force Convection-permitting model (CPM) simulations at kilometer-scale that give a downscaled and improved representation of hourly precipitation extremes (Chan et al., 2020). Convection Permitting Models (CPMs) represent a significant advancement in the representation of atmospheric convection at the temporal and spatial scales critical for driving changes in intensity, frequency, and clustering of extreme precipitation, which is important for flood generation (Chan et al., 2014; Fosser et al., 2024; Fowler, Lenderink, et al., 2021; Kendon et al., 2012; Prein et al., 2015). These kilometer-scale variations in extreme precipitation play a critical role in the generation of fluvial floods (Paschalis et al., 2014; Peleg et al., 2020), and ensembles of climate projections from CPMs provide an opportunity to assess future changes to flooding in catchments and estuaries (Archer et al., 2024; Orr et al., 2021; Rudd et al., 2019). CPMs capture storm characteristics and are used to force hydrological models to simulate river flows and future risks under climate change (Kay et al., 2019).

In addition to dynamical downscaling of hydrological processes, Tinker et al. (2024) developed a set of Northwest European Shelf (NWS) marine climate projections. The 12 UKCP18 GCM-PPE members, also based on HadGEM3-GC3.05, were downscaled with the 7 km shelf seas version of NEMO 4.04 (Coastal Ocean version 9,

CO9) (Tinker et al., 2020). Simulations represent the state of the art for Northwest Shelf marine projections (Tinker et al., 2024), and directly simulate the multitude of atmospheric-ocean processes that affect coastal and estuarine flood hazard at relevant temporal and spatial scales, from local effects of wind waves to tides and the inverse barometer effect (Ponte et al., 2019). By providing high-resolution projections, these models enable robust assessments of how evolving oceanographic and storm conditions, including SLR and extreme weather events, may amplify coastal flooding risks (Jevrejeva et al., 2024). This comprehensive downscaling approach demonstrates the potential for more accurate assessments of climate change impacts on extreme precipitation, river flows, and sea level, crucial for assessment of future compound flooding.

The research here demonstrates a step change in capacity to estimate future compound flood behavior in estuaries. For the first time, we use multiple ensembles of hourly and sub-mesoscale, physically consistent, hydrological and marine projections that allow us to diagnose future changes to compounding flood conditions. Projections of future storm surges and river discharge have been used to assess changes in the magnitude and timing of storm-driven compound events. The Dyfi Estuary, west Wales, UK, was chosen as a test case due to the availability of data and documented evidence of past compound storm events, such as Storm Ciara in February 2020 (Harrison et al., 2021; Lyddon et al., 2022; Robins et al., 2021). The use of PPE simulations means that model uncertainty of GCMs can be included and combined with return level uncertainty specific to each ensemble member. The study aims to identify how the timing and magnitude of extreme storm-driven compound events will change in the future, providing crucial insights for future incident and hazard management strategies to determine whether these events will become problematic, and how best to prepare for them. Section 2 provides an overview of the data sets, compound flood indicators, and a hydrodynamic model applied here to assess future changes in compound flooding. The results identify the magnitude of change in drivers of storm-driven compound flooding, future changes in dependence and characteristics of flood inundation and depth in the Dyfi Estuary.

2. Methods

2.1. Case Study

The Dyfi Estuary is studied here due to the availability of long observational timeseries to assess temporal changes in the magnitude, timing, and behavior of storm-driven compound events. There is a long instrumental record of sub-daily river discharge measurements at the head of the estuary, sea level measurements near the estuary mouth, and the availability of hourly projections of river discharge combined with hourly projections of sea surface height (SSH) and residual surge—both driven by the same GCM-PPE. The Dyfi estuary is located on the west coast of Britain, has a mean surface area of 17 km^2, is approximately 15 km long, and is relatively shallow, largely drying out at low tide (Robins & Davies, 2010; Shi, 1993). The estuary is macro-tidal with a mean spring tidal range of ∼5 m. The River Dyfi is the primary fluvial input to the estuary, draining a steep mountainous catchment area of 470 km^2 and having a length of 48 km with an annual mean discharge of 23 m^3/s and extreme 95th flow of 78 m^3/s (Robins et al., 2021). These scales imply that fluvial flood waters will reach the Dyfi Estuary in a matter of hours. Previous research has shown compound flooding is likely to occur in this estuary (Harrison et al., 2021; Lyddon et al., 2022; Robins et al., 2021) due to the high number of storms per season, the aspect of the estuary (facing prevailing storm tracks from the Atlantic), and the steep catchment shape with short runoff transmission times. Indeed, the Dyfi Estuary has experienced compound flooding, notably on 18 November 2009 (0.77 m skew surge occurred within 5 hr of a 382 m^3/s discharge) and 11 February 2002 (0.54 m skew surge occurred within 15 min of a 337.7 m^3/s discharge), in both cases causing widespread flood damage and road closures (Griffith et al., 2020). A national characterization of compound flood drivers by Lyddon et al. (2022) shows the Dyfi to be typical of ∼25 estuaries on Britain's west coast that are similar in scales and driver behavior.

2.2. Instrumental Data

The NTSLF Class A tide gauge located at Barmouth, 20 km north of the mouth of the Dyfi Estuary, was used as a record of observed total water level and residual storm surge (total water level – predicted tide). The tide gauge record is available from 1 January 1991–31 December 2021 at 15-min resolution. The record was processed to remove flagged data (error or modeled data) to leave only actual observed data. This produced a record with 66% data coverage, with no data available since January 2016. Observed river discharge measurements are available at 15-min resolution at Dyfi Bridge (gauge number: 64001; location: 52.60°N, 3.85°W) from 1 January 1970–1

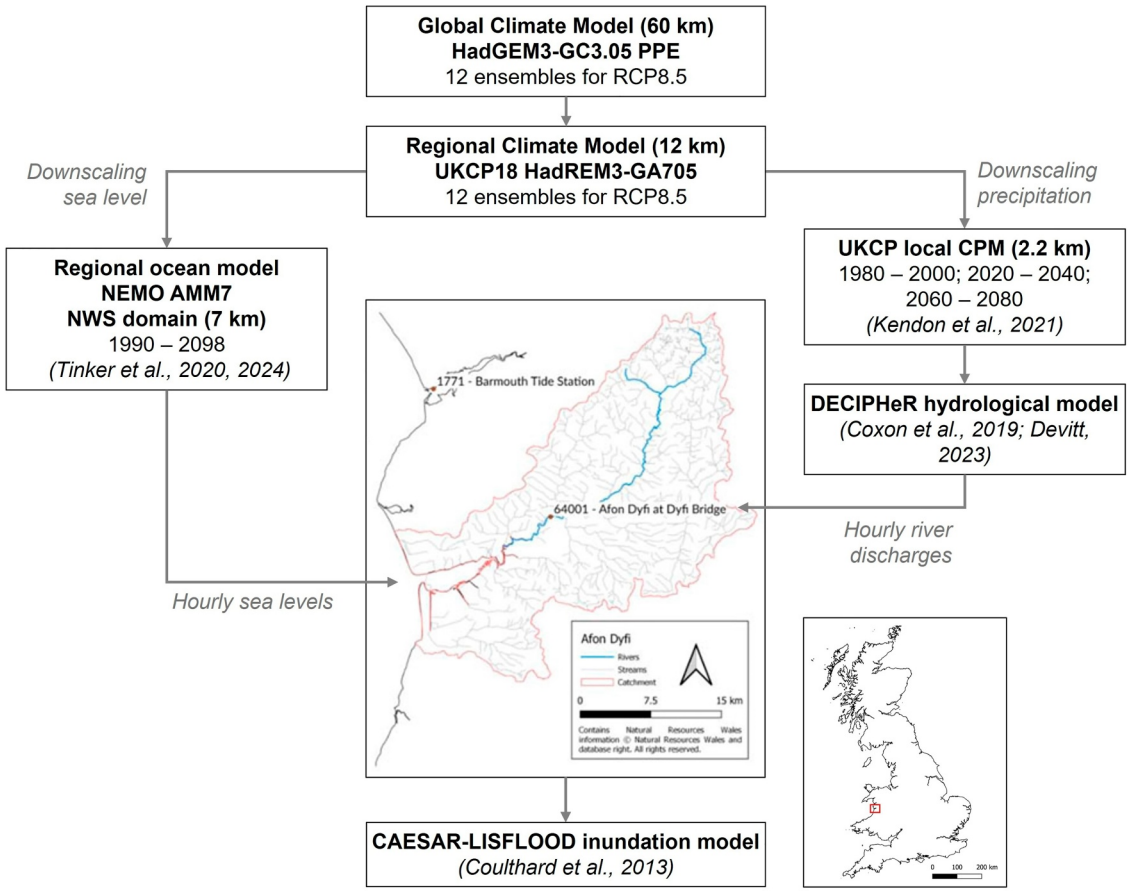

Figure 1. Framework showing downscaled fluvial and marine projections used here for the Dyfi Estuary, west Wales.

December 2021 (NTSLF, 2022). This is the most downstream, non-tidal river gauge in the catchment, and the record has 87% data coverage.

2.3. Future Projections

Future projections of river discharge and sea level were driven by the 60 km HadGEM3-GC3.0 GCM (Figure 1). The projections comprise 28 global PPE ensemble members, formed by varying uncertain parameters within the model physics, including global carbon and sea ice, allowing uncertainty in future projections up to 2100 to be explored systematically (Sexton et al., 2021; Williams et al., 2018). These marine and fluvial projections were run under the Representative Concentration Pathway (RCP) 8.5, corresponding to a high-emissions climate change scenario where greenhouse gas emissions continue to increase into the 22nd Century. Despite being recognised as a low-likelihood scenario, RCP8.5 has a high signal-to-noise ratio so climate response can more easily be separated from internal variability and is valuable for risk-based decision-making as it provides a comprehensive view of potential future risk (IPCC, 2021; Tinker et al., 2024). 12 ensemble members of the RCP8.5 GCM-PPE (see Table 1) were downscaled to the 12 km Regional Climate Model (RCM) simulations over the northwest European shelf as part of the UK Climate Projections project (Tucker et al., 2021)–termed UKCP18 RCM-PPE. For atmospheric processes, the RCM simulations were downscaled to a 2.2 km CPM, used to simulate small scale behavior seen in the atmosphere, in particular convection-permitting precipitation (Kendon, Fosser, et al., 2021; Murphy et al., 2018). For marine processes, the RCM simulations were downscaled to a 7 km regional ocean model (NEMO 4.04 (Coastal Ocean version 9, CO9), run on the Atlantic Margin Model 7 km grid (AMM7)), used to simulate small scale behavior seen in the NW European shelf sea hydrodynamics, in particular storm-driven surge-tide propagation (Tinker et al., 2020, 2024). From these models, hourly continuous climate data was used to force marine and hydrological models to provide projections of changes in each driver of storm-driven compound flooding. This is the first time that hourly and fine spatial resolution (7/2.2 km sea level/

Table 1
Normalized Bias to Show How Many Standard Deviations the Observed 20-Year Mean (Sea Level: Barmouth, River Discharge: Afon Dyfi at Dyfi Bridge) Is From Each Modeled 20-Year Ensemble Mean (Sea Level: NEMO CO9, River Discharge: Decipher)

Ensemble	0000	0605	0834	1113	1554	1649	1843	1935	2123	2242	2305	2335
NEMO CO9	−0.18	−0.57	−0.25	0.02	0.37	−0.14	0.43	−0.1	0.22	−0.49	0.57	0.11
Decipher	−0.29	−0.02	0.49	0.07	0.3	0.14	0.21	−0.36	0.02	−0.26	0.43	−0.73

Note. Less than 2 is considered acceptable.

precipitation), physically consistent, climate projections are used to assess changes in storm surge and river discharge-driven compound events.

2.3.1. Marine Projections

Marine data at the mouth of the Dyfi Estuary was accessed from the Met Office Managed Archive Storage System archive on JASMIN, via the Met Office Operational Storage Environment interface. Monthly output files contained data at hourly resolution, spanning 1990–2098, for 12 ensembles (listed in Table 1). As stated in Tinker et al. (2024), there were a series of files that were not archived correctly, as shown in Table S1 in Supporting Information S1. Tinker et al. (2024) recommended recreating missing files by averaging the daily mean files; however, this approach would result in the loss of sub-daily temporal resolution. An alternative method involves averaging data from the same month of the previous and following years. This latter approach, which was used in this study, maintains the seasonal cycle and any trends in the data, though it may affect some statistics, such as estimates of interannual variability. Although NEMO CO9 includes a wetting and drying module to account for realistic coastal bathymetry and coastal processes, caution is advised when using model outputs within three grid boxes of the land. Consequently, manual processing and qualitative checks were performed to ensure that coastal grid boxes are "wet." Projections were taken from position 52.534, −4.111, located one grid cell from the coast and at the mouth of the Dyfi Estuary. It is important to note that while the oceanographic SLR is included in the forcing GCM, this model does not fully account for other SLR aspects such as tectonics and ice dynamics, and thus should not be considered a comprehensive SLR model. Total water level time series were de-tided using a Doodson filter, which is a bandstop filter for frequency bands including diurnal, semi diurnal, 8 hr, 6 hr, to generate a residual storm surge. Separating the residual storm surge from the modeled total water level gives a tide only signal. The Doodson filtering approach yields a residual that is not identical to the surge derived from harmonic tide–subtraction of observed total water level, and therefore the two signals may differ subtly in amplitude and timing, though both capture the storm surge variability on multi-hour to multi-day timescales.

To assess the performance of AMM7 in reproducing the magnitude of storm surges, it is important to appreciate that GCMs are not designed to replicate the observed phase of weather events, making direct comparison of high-resolution time series unrealistic. Instead, the climate is evaluated by comparing long-term statistical records of observations with model outputs. SLR was first retained in the modeled simulations to reflect any changes captured in the tide gauge record. The observed 20-year mean (1991–2011, with 78% data coverage) was calculated and compared with the modeled 20-year mean for each ensemble member (1990–2080). As per Tinker et al. (2024), an offset of 0.85 m was calculated to align observations and projections: the difference between the NWS-PPE ensemble mean and temporal mean and tide gauge temporal mean for the common overlap period. All analysis is presented with this offset applied. A normalized bias was calculated to determine how many standard deviations the observed 20-year mean deviates from the ensemble mean of the PPEs. If the normalized bias was less than 2, the observations are within 2 standard deviations of the ensemble mean, indicating that the PPE is consistent with the observations. The ±2 range is intended to show that the observed surge generally falls within the modeled variability, indicating that the PPE captures realistic surge behavior over time.

$$\text{Normalized Bias} = \frac{\text{Ensemble mean} - \text{observed mean}}{\text{Ensemble standard deviation}} \quad (1)$$

The comparison of ensemble annual means to observation annual means follows the approach used by Tinker et al. (2024) (Figure 6, pp. 848). Tinker et al. (2024) demonstrated good agreement between observations and

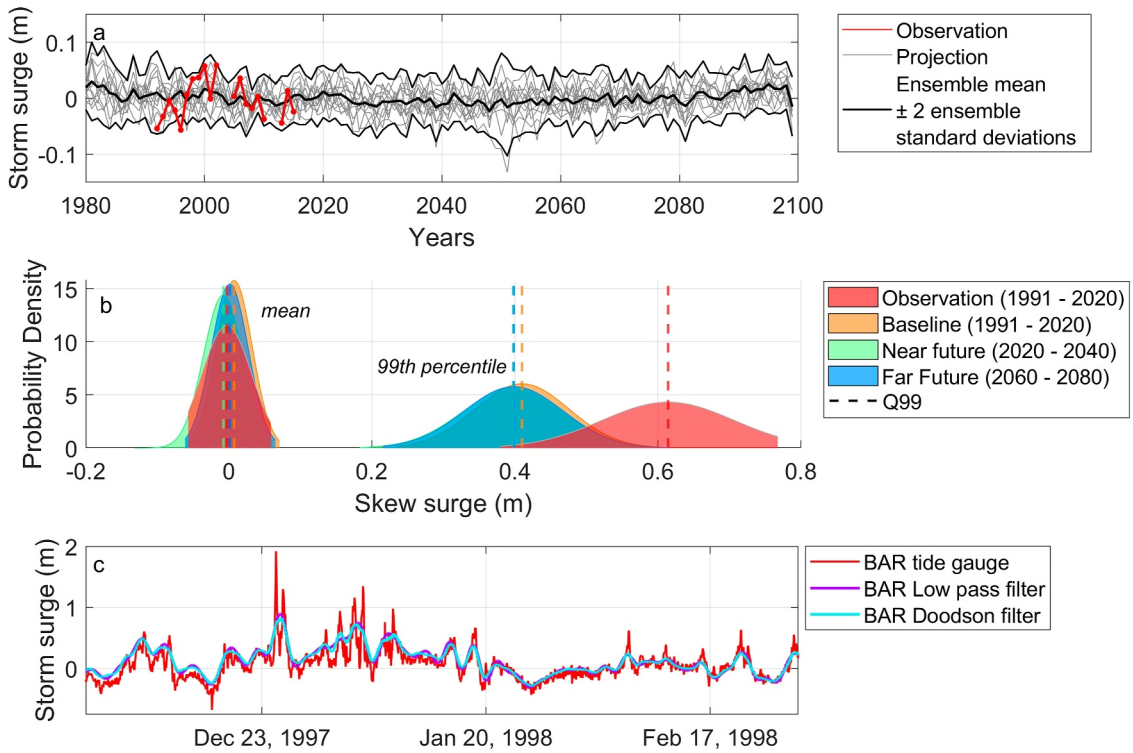

Figure 2. (a) Comparison of time series of annual mean storm surge from Barmouth tide gauge (red) and 12 ensemble members (gray), with the ensemble mean ± 2 ensemble standard deviations shown in black. (b) Normal distribution fitted to annual mean (left) and 99th percentile (right) storm surge from Barmouth tide gauge (red), and 12 ensemble members grouped in three time slices (gray to white) with mean (dashed line). (c) Doodson (blue) and low pass (purple) filter applied to observation tide gauge data (red) to assess influence of filtering process on magnitude of residual surge.

model ensembles at Holyhead approximately 100 km north of the Dyfi. This method is now applied to the Barmouth tide gauge, 20 km north of the Dyfi, and baseline projections from a grid cell close to the tide gauge, offshore from the River Mawddach for a 20-year period of overlapping data (1990–2020) where more than 50% of observation data exists in the record to maximize data for comparison. Similarly, the method is applied to a 20-year overlap period with river gauge data (1980–2000), from Dyfi Bridge (gauge number: 64001) and baseline hydrological projections. Table 1 shows a strong agreement between the annual mean storm surge from the Barmouth tide gauge and the ensemble mean, and annual mean river discharge and the ensemble mean. For all ensembles, the normalized bias was less than 2, indicating that the PPE is consistent with observations. This analysis has been extended to a range of percentiles (25, 50, 75, 95, 99th) and also applied at Fishguard tide gauge, located 80 km southwest of the Dyfi Estuary, which has a longer record of complete data (1980–2021), all showing normalized bias within 2 to illustrate model agreements (Tables S2–S4 in Supporting Information S1).

The modeled and observed storm surge data include a component of SLR, which was removed by subtracting linear regressions of the long-term trends. The resulting detrended modeled and observed storm surge was used for all subsequent analyses. The comparison of detrended ensemble annual means to observation annual means shows good agreement in Figure 2a. The ensemble mean is less variable than the observations and individual ensemble members, and variance of each individual baseline ensemble member (0.016–0.02 m) is consistent with the observation (0.023 m).

The observed annual mean, 25, 50, 75, 95, and 99th percentile storm surge over a 21-year period was calculated from tide gauge data and each ensemble mean. A normal distribution was then fitted to these values for each ensemble to interpret the spread within each model's projections and identify ensembles that may predict more or less extreme outcomes (Figures S1 and S2 in Supporting Information S1). The distributions were then averaged across all ensembles (Figure 2b) to smooth out variability from individual models and emphasize broader trends and robustness. Results for the mean and 99th percentile are only shown here. Combining the ensemble means and variance of individual normal distributions into one averaged distribution makes it easier to understand the

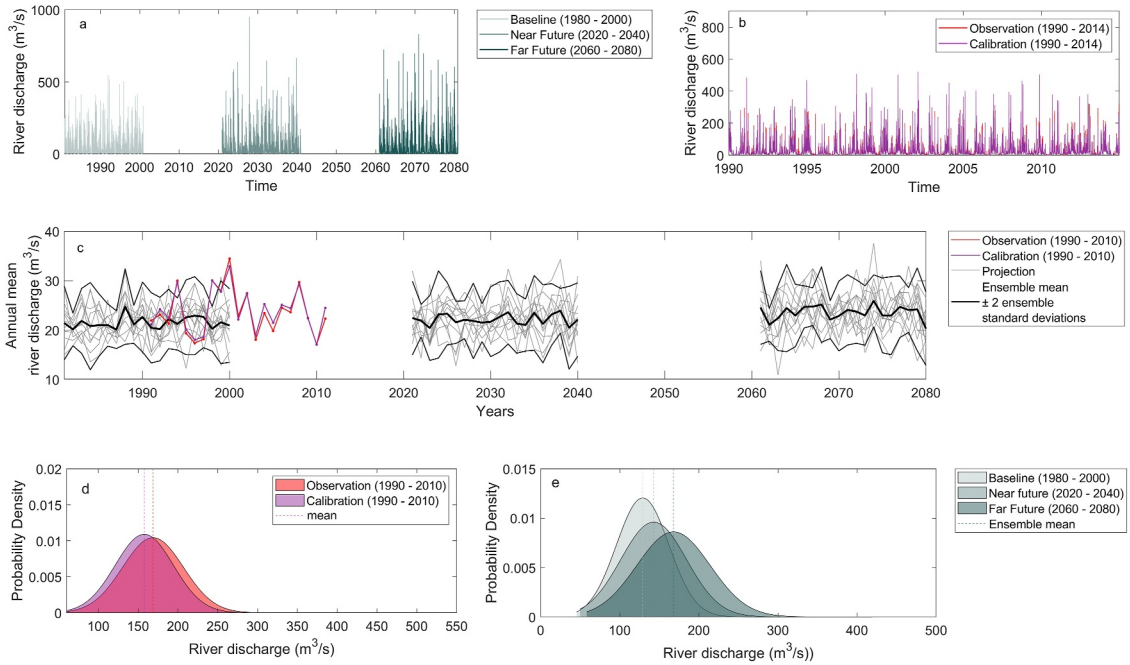

Figure 3. Fluvial projections showing (a) time series of projected discharge across the baseline, near future and far future time slices; (b) time series of observational (red) and model calibration (purple) discharge for 1990–2014; (c) annual mean discharge averaged across observational (red) and model calibration (purple) data for 1990–2014, and annual mean discharge across the 12 UKCP18 Local ensembles (gray lines) for the baseline, near future and far future time slices, with the ensemble mean ± 2 ensemble standard deviations (black lines); (d) normal distributions fitted to the annual 99th percentile discharge for the observational and calibration data; and (e) normal distributions fitted to the annual 99th percentile discharge across the 12 ensembles for the baseline, near future and far future time slices. See Figure S2 in Supporting Information S1 for distributions of each ensemble run and averaged.

collective characteristics of the ensemble. A probability density function fitted to the mean for modeled and observed data shows good agreement, centered around 0 m. The mean observed 99th percentile (0.61 m) is higher and the tails longer than the projections across three time slices. To demonstrate how the filtering process in the projections can dampen extremes in surge magnitudes, the same Doodson filter that is applied to total water level from AMM7 is applied to the Barmouth tide gauge total water level, alongside a Chebyshev Type II low pass filter as an additional example. Figure 2c illustrates that after detrending the modeled surge data, the Doodson filter acts as a bandstop filter for the main frequency bands (diurnal, semi-diurnal, 8-hr, 6-hr), effectively reducing the peaks. The Doodson method removes some higher frequency surge behavior and depresses the magnitude of storm surge peaks, with the low pass filter producing a similar result. Although the AMM7 model does not fully capture higher frequency surges, the simulations are sufficiently realistic and suitable for analyzing compound events. These simulations provide extensive data: 100 years of continuous hourly resolution over 12 ensemble members, generated from the same GCM that produces hourly river discharge projections.

2.3.2. River Discharge Projections

The 12 member UKCP18 RCM-PPE were downscaled to a 2.2 km resolution CPM (termed UKCP18 Local) for three time periods: baseline (1981–2000), near future (2021–2040) and far future (2061–2080) (Kendon et al., 2019; Kendon, Prein, et al., 2021; Murphy et al., 2018) (Figure 3a). Uplift analysis of outputs from UKCP18 Local show an intensification of summer hourly precipitation compared to the driving RCMs (Chan et al., 2023). DECIPHeR, a hydrological model (Coxon et al., 2019), was used to simulate river discharge in the Dyfi catchment, to allow for realistic representation of rainfall intensity and storm duration (Devitt, 2023). To parameterize the hydrological model, 10,000 simulations were performed with within a Monte Carlo simulation framework with parameter sets randomly sampled from a wide parameter space. Calibration simulations were forced with hourly observational rainfall (CEH-GEAR 1 hr, Lewis, Quinn, et al., 2019) and potential evapotranspiration (CEH McGuinness-Bordne; Tanguy et al., 2018) for the period 1990–2014. Both observational data products were regridded from their native 1 km resolution to 2.2 km to match UKCP18 Local. Calibration simulations were evaluated against observed hourly river flow data (Figure 3b) using Nash-Sutcliffe Efficiency

(NSE; Nash & Sutcliffe, 1970) and Kling-Gupta Efficiency (KGE; Gupta et al., 2009) analyses. The NSE and KGE scores for the best performing parameter sets were 0.82 and 0.79. DECIPHeR was run continuously to simulate hourly discharge for all 12 ensemble members using the top 100 model parameterizations with the UKCP local data during the baseline, near future, and far future time slices. The UKCP18 Local precipitation was not biased corrected as it was found to agree well with hourly rainfall observations. UKCP18 Local has no explicit PET data, and so PET was derived from hourly temperature data using the same PET equation (McGuiness-Bordne) as is used by the observational data in the calibration simulations. Discharge projections were extracted at the location of the Dyfi Bridge river gauge (52.6, −3.85), at the head of the estuary (15 km up estuary from the mouth). Further details of the hydrological modeling procedure are provided by Devitt (2023).

Extensive calibration of DECIPHeR has been undertaken (Coxon et al., 2019) and robustness of river discharge projections at the Dyfi tested (Devitt, 2023). For completeness, the methodology applied to show the reliability of the marine projections was applied to the best performing hydrological parameter set. The methodology was applied to one hydrological set only to reflect the resolution of data that is available for the marine data. A normalized bias was calculated per ensemble member between the overlapping data (1990–2000) from the 12 ensemble members of the baseline time slice and the river gauge (Table 1). All show a bias under 2 indicating good agreement. An offset, the difference between the UKCP18 Local CPM ensemble mean and river gauge temporal mean for the common overlap period, is also calculated and applied (0.34 m^3/s), and annual mean river discharge across 12 ensembles shows good comparison with observation gauge data (Figure 3c).

A normal distribution was fitted to annual 99th percentile for every hydrological simulation, and averaged for each ensemble (see Figure S3 in Supporting Information S1), and then averaged across all ensembles for each time slice to understand how well the hydrological models perform (Figures 3d and 3e). Figure 3d shows normal distributions fitted to the observational and calibration runs, and Figure 3e shows normal distributions for the concatenated baseline, near future and far future simulations from the best performing parameter set. The baseline simulations vary from near future and far future simulations in terms of peakedness and magnitude, with smaller variance. The variance of each individual baseline ensemble member (520–975 m^3/s) is consistent with the observation (1,019 m^3/s). This gives confidence when using outputs from the hydrological models to understand future changes in river discharge.

2.4. Future Changes in Compound Events

2.4.1. Changes in Magnitude and Return Periods of Skew Surge and River Discharge

Sea level and river projections were first analyzed individually, to identify future changes in means, quantiles, outliers, and return periods for each driver. For river projections, quantiles were calculated for each complete 20-year time slice (1980–2000, 2020–2040, 2060–2080) across all hydrological runs and ensemble members. Means, quantiles, and outliers were calculated for each of the 100 best performing hydrological runs, for 12 PPEs. The 100 hydrological runs were then averaged across the 12 PPEs, and then averaged across each time slice. Boxplots show quantile range, mean, and maximum outliers (Figures 6 and 8).

Similarly, quantiles and means were calculated for each of the 12 storm surge PPEs and averaged for each time slice. Skew surge was calculated from the storm surge projections, which is defined as the difference between maximum observed and predicted high tide within a 12-hr tidal cycle (Batstone et al., 2013). Skew surge has been used as a more representative measure of dependence between extreme sea level and river flow, across Europe (Camus et al., 2021; Hendry et al., 2019; Paprotny et al., 2018) and the USA (Jane et al., 2022; Moftakhari et al., 2019), and a more useful metric for flooding (Haigh et al., 2016). Despite the first 10 years of marine projections defined as "spin up," 1980–1990 projections are still used here for comparison with river discharge also simulated for this time slice. This is acceptable here as the model is able to "spin up" quicker for barotropic conditions (e.g., storm surge), but would require longer for baroclinic processes (e.g., salinity and temperature).

Return periods of the magnitudes of 1/2-year up to 1/50-year skew surge and river discharge events, unique to each ensemble member, were calculated. Previous research has concatenated individual ensembles to give 240 years of data (12 × 20-year time slices) (Archer et al., 2024), which does not explicitly account for uncertainty associated with each ensemble member. The approach used here is based on Chan et al. (2023) which handles each ensemble separately to acknowledge that each PPE represents different parameterizations with its own uncertainty. For the river discharge data, each set of 100 hydrological runs was treated separately across the 12

ensembles. 20-year annual maxima (A_{MAX}) for each hydrological run was identified to generate 100, 20-year A_{MAX} time series. These time series were concatenated to give a 2000-year data set from which 1/2-year to 1/50-year return periods were calculated for each ensemble (Figure S3 in Supporting Information S1). For skew surge data, one 110-year time series of A_{MAX} was generated per NEMO AMM7 ensemble member. We used bootstrap resampling of the A_{MAX} for each of three 20-year time slices respectively, to produce 100 resampled 20-year series for each ensemble. Histograms were used to test if the 100 resampled A_{MAX} set is from the same distribution as the original ensemble member. As for fluvial projections, the 100, 20-year A_{MAX} time series were then concatenated into a 2000-year data set (Figure S4 in Supporting Information S1). Return levels corresponding to different return periods were estimated using the Gumbel distribution, which is a commonly applied extreme value distribution for modeling annual maxima, across 12 ensembles for each 20-year time slice. For each ensemble, the annual maximum values representing the sampling distribution of extremes, from which sample mean and standard deviation were calculated.

Return levels Q_T for return periods $T = 2$ to 50 years were calculated using the Gumbel reduced variate:

$$y_T = -\log\left(-\log\left(\frac{T-1}{T}\right)\right)$$

These values were standardized using the ensemble mean and standard deviation of the reduced variate distribution (y_n, s_n), and scaled to the data distribution:

$$Q_T = \bar{x} + \left(\frac{y_T - y_n}{s_n}\right) \cdot \sigma$$

This method provides an ensemble-based estimate of return levels, accounting for model variability.

2.4.2. Changes in Dependence and Timing of Compound Events

Whilst the GCM does not simulate weather events, the same atmospheric conditions in each PPE will cause extremes in both the storm surge residual (and skew surge) and precipitation (and subsequently river discharge). The following analysis shows how changes in atmospheric conditions will cause changes in the co-occurrence of extreme skew surge and river discharge that cause compound flooding.

The best performing parameter set for river discharge projections was used to limit the analysis to one set of 12 PPE projections. A peaks-over-threshold analysis (Lyddon et al., 2022) identified peaks in discharge that exceeded a moving threshold of the data for each ensemble (calculated based on a 3-month moving mean + 50th percentile of each 20-year time slice) (red circles in Figure S4 in Supporting Information S1). The hydrograph storm window, based on the average hydrograph duration (1984–2013) is 20.42 hr for the River Dyfi (Lyddon et al., 2022). The largest skew surge within the hydrograph storm window, that is, within 10.21 hr before and after the peak in river discharge, was identified (red crosses in Figure S5 in Supporting Information S1). We assessed the dependence between the peaks in river discharge and associated peaks in skew surge using Kendall's rank correlation coefficient (using two-way sampling). This standard measure of dependence has been used in previous studies (Hendry et al., 2019; Lyddon et al., 2022; Marcos et al., 2019; Wahl et al., 2015; Ward et al., 2018), and provides information about dependence when one driver is extreme but not necessarily the other. To investigate the frequency the most extreme compound events, where extreme discharge has occurred at the same time as an extreme skew surge, the mean number of times per storm season (June–May) that peak river discharge and associated skew surge both exceeded the 95th percentile was identified (Lyddon et al., 2022). The above analyses provide insight on the dependence (or lack of dependence) between the drivers of compound flooding. Further, the average time lag between extreme peak river discharge and skew surge (95th percentiles) was calculated.

2.4.3. Multi-Variance Extreme Value Analysis (Extreme Dependence Measure)

In addition to using Kendall's rank correlation coefficient, extremal dependence using tail dependence coefficients was used to characterize joint behavior of compound events when both drivers were extreme. Following the peaks-over-threshold analysis described above, the probability of extreme compound events, where both peak river discharge and associated peak skew surge exceeded the respective 95th percentile, was calculated for

baseline, near future and far future simulations. The extremal dependence measure $\chi(u)$ (Coles et al., 1999) was calculated for each set extreme discharge and skew surge peaks to investigate the level of dependence in tail behavior using different thresholds ($q = 0.1$–0.99). Results are presented as ensemble means, and the coefficient χ represents the probability of one variable being extreme (exceeding a threshold q), given that the other variable is extreme (exceeding the same threshold q). If one variable exceeds a certain extreme threshold (percentile), then the value of χ represents the risk that the other variable will also exceed that extreme threshold (Defra/Environment Agency, 2005; Svensson & Jones, 2002, 2004). If all of the extreme occurrences of two variables exceed a given threshold at the same time, this indicates total dependence ($\chi = 1$). If all the extreme occurrences of one variable exceed a given threshold but all of the second variable do not, this indicates total independence ($\chi = 0$).

2.5. Inundation Modeling Future Compound Flooding

To explore how changes in drivers of compound events impact the degree of flooding in the Dyfi estuary, the LISFLOOD-FP hydrodynamic model (Bates et al., 2010) was used within a sensitivity test framework. A series of idealized compound events were simulated, parameterized on river and sea level conditions that are representative of the baseline, near future, and far future time slices (see Section 2.3) to identify how changes in drivers of compound flooding change the degree of flooding in the Dyfi estuary. LISFLOOD-FP uses a flow-routing algorithm that determines the direction of flow based on the elevation gradient and conserves mass and partial momentum (Bates et al., 2010; Coulthard et al., 2013). We identify areas that have a higher chance of flooding under future conditions, presented as a series of flood hazard maps.

2.5.1. Model Setup and Calibration

The LISFLOOD-FP model domain extended from the Dyfi Bridge river gauge station in the northeast, to an ocean boundary to the west of the estuary mouth (longitude: −4.10), and south to cover the low-lying flood plains of the catchment (latitude: 52.47). The production of the digital elevation model (DEM) of the bathymetry of the Dyfi estuary and elevation of surrounding land was performed by using multiple data sources (see Supporting Information S1 for further details). All elevation data were corrected to Ordnance Datum Newlyn (ODN) and merged into a regular grid with a spatial resolution of 20 m. A DEM with 20 m grid cell size has been shown to be optimal for flood modeling of medium to small size estuaries (Harrison et al., 2021; Seenath, 2018) without compromising on computational efficiency. LISFLOOD-FP was run in reach mode, in which the model is forced with river discharge and water level time series at the upstream (river) and downstream (offshore) boundaries, respectively. For model calibration, gauged time series of river discharge and sea level were used, outlined in Supporting Information S1, and refer to Barada et al. (2022) for further details.

2.5.2. Idealized Model Scenarios

A set of LISFLOOD-FP simulations were performed with idealized sea level and river discharge boundary conditions to show how projected climate changes this century will influence flood inundation in the Dyfi Estuary. In total, 14 distinct simulations were performed, each lasting 3 days, that combine river discharge concurrently with storm surge superimposed on an idealized tide at levels representative of 1/20-year and 1/50-year return period events for baseline, near future, and far future time slices derived from the marine and hydrological projections, including UKCP18 SLR projections (Table 2). The simulations allow for model spin-up, thus allowing the assumed initial condition to become consistent with the hydrodynamic system, and with peak water level and peak discharge occurring after ∼40 hr (Figure 4). Two baseline simulations were initially run, representing 1/20-year (termed "B20") and 1/50-year (B50) compound events. Next, six near future events were simulated, three for 1/20-year events no SLR (N20_noSLR), with SLR projected by a "low emissions" future RCP2.6 (N20_minSLR), and with SLR projected by a "high emissions" future RCP8.5 (N20_maxSLR), and three similarly for 1/50-year events (N50_noSLR, N50_minSLR, N20_maxSLR). Finally, these six scenarios were repeated for the far future time slice (F50_noSLR, F50_minSLR, F20_maxSLR, F50_noSLR, F50_minSLR, F20_maxSLR) (Table 2). The boundary conditions for these 14 simulations were created as per Lyddon et al. (2024, Section 2.5) and are described in more detail below.

To characterize river discharge behavior, a two-parameter gamma distribution was used to generate a synthetic series of normalized, idealized gamma curves that represent hydrograph shapes that cover the natural range of river flow behaviors experienced in the Dyfi based on 30 years of river discharge data from the Dyfi Bridge river gauge

Table 2
LISFLOOD-FP Flood Inundation Simulations for the Dyfi Estuary, Showing Return Period, Time Slice, Q, S, and Sea-Level Rise Projection Used

Run	Return period	20-year time slice	Peak river discharge (m^3/s)	Peak skew surge (m)	SLR projection (m)
B20	1/20-year	Baseline	617	0.71	0
N20_noSLR	1/20-year	Near-future	667	0.72	0
N20_minSLR	1/20-year	Near-future	667	0.72	0.21 (RCP2.6)
N20_maxSLR	1/20-year	Near-future	667	0.72	0.39 (RCP8.5)
F20_noSLR	1/20-year	Far-future	797	0.74	0
F20_minSLR	1/20-year	Far-future	797	0.74	0.21 (RCP2.6)
F20_maxSLR	1/20-year	Far-future	797	0.74	0.39 (RCP8.5)
B50	1/50-year	Baseline	731	0.79	0
N50_noSLR	1/50-year	Near-future	790	0.8	0
N50_minSLR	1/50-year	Near-future	790	0.8	0.27 (RCP2.6)
N50_maxSLR	1/50-year	Near-future	790	0.8	0.72 (RCP8.5)
F50_noSLR	1/50-year	Far-future	937	0.82	0
F50_minSLR	1/50-year	Far-future	937	0.82	0.27 (RCP2.6)
F50_maxSLR	1/50-year	Far-future	937	0.82	0.72 (RCP8.5)

Note. Row colours correspond to flood scenario in Figure 8 and Figures S12–S25 in Supporting Information S1.

(see Lyddon et al., 2024; Robins et al., 2018). Next, the gamma curve with the gradient of the rising hydrograph limb that most closely resembled the average gradient of the top 100 most extreme events analyzed in Lyddon et al. (2022) was selected. The selected idealized hydrograph had the largest gradient representing the flashiest flow behavior. Finally, the magnitude of the idealized hydrograph was scaled to a peak discharge representative of 1/20-year and 1/50-year return levels, with a base flow of 20 $m^3\ s^{-1}$ which represents mean flow conditions (Table 3).

Total water level time series were created using idealized tidal signals combined with residual surges. First, a sinusoidal elevation with a period of 12.42 hr (equivalent to the dominant M2 tidal constituent) was parameterized

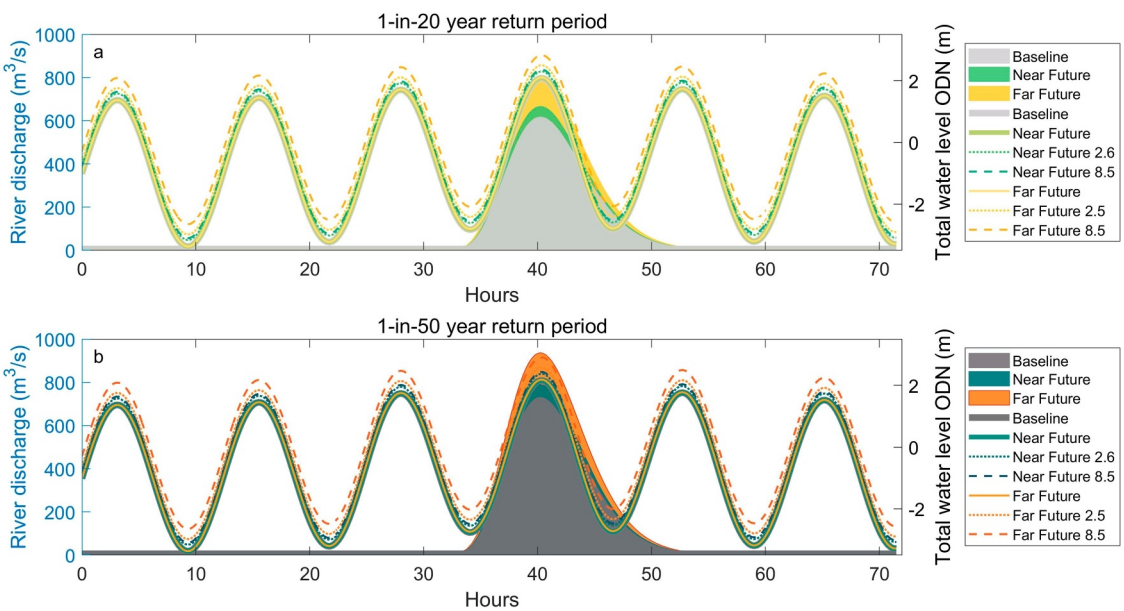

Figure 4. Boundary conditions for LISFLOOD-FP simulations showing river discharge (left axis) and sea level (tide + surge and sea-level rise (SLR), right axis) for (a) 1-in-20 and (b) 1-in-50 years return period under baseline, near future and far future scenarios (solid curve) with the additional of SLR under RCP2.6 (dotted curve) and RCP8.5 (dashed curve).

Table 3
1/20-Year and 1/50-Year Return Period Magnitudes (Q) Used to Scale Idealized Hydrograph

	1/20-year			1/50-year		
	Baseline	Near future	Far future	Baseline	Near future	Far future
Q (m^3/s)	617	667	797	731	790	937
S (m)	0.71	0.72	0.74	0.79	0.8	0.82

to represent mean tides at Barmouth, determined using a harmonic analysis (T-Tide, Pawlowicz et al., 2002), based on 12 months of tide gauge data from Barmouth (2002–2003). This experimental design purposely neglected the influence of other constituents so that the results were standardized. The model simulated the shallow-water propagation of the tide advancing up the estuary. Second, a residual surge was added to the tidal elevation time series to represent the meteorological contribution to the total water level. The shape of the surge was representative of typical storm conditions for Barmouth (Environment Agency, 2018). The surge was shifted in time so that the maximum surge height coincided with the fourth high tide (at around 40 hr), which was also the timing of peak discharge. The surge was scaled to the magnitude of a 1/20- and 1/50-year return period surge, for each time slice (see Table 2). The representative surge curve has a standard duration of 100 hr which was maintained across all simulations so changes in flood inundation could be attributed to changes in surge magnitude. The resultant 3-day time series represented several tidal cycles where flooding was not expected (tide-only), followed by a tide + max surge event at ∼40 hr, before the regular tidal cycles resumed. The peak total water level had a 0 hr time lag with peak in river discharge to represent a concurrent compound flood event. Further studies could consider the sensitivity of flooding to different time lags. Finally, for the SLR scenarios, an increase in water level was added in line with expected levels during each time slice (Table 2). Annual average 50th percentile SLR projections under RCP2.6 and RCP8.5 climate change scenarios were obtained from the grid cell closest to the Dyfi Estuary, from the publicly available UKCP18 21st century time-mean sea level projections (Met Office Hadley Centre, 2018). The RCPs used represent a more and less extreme emissions projections. Low-emission scenario, RCP2.6, which represents limiting warming and stronger mitigation efforts, is used as an indicator of higher likelihood, lower severity SLR.

2.5.3. Simulations of Flooding

The following methodology was applied to identify the extent of flood extent under each scenario. *FloodArea* quantifies the inundation area (km^2) of the Dyfi estuary floodplains as a function of river discharge, total water level, and sea level drivers. *FloodArea* was compared between the 14 simulations. The output data comprise water depth grids in time layers with an interval of 15 min. Percentage increases in *FloodArea* between simulations and maximum modeled water surface elevations along the deepest channel of the estuary were calculated, and spatial inundation maps were presented.

3. Results

3.1. Future Changes in Skew Surge

Projected changes in magnitude of skew surges at the Dyfi Estuary, based on the RCP8.5 "high emissions" scenario across 12 ensembles, is shown in Figure 5a for three time slices (baseline, near future, far future). Median skew surge of the projections (all three time slices) remains in line with current observations, at ∼0 m. Removing the sea level trend shows that skew surge is unlikely to change significantly up to the end of the 21st century. The 75th percentile skew surge remains between 0.28–0.29 m, and there is also little variability (a few centimeters) in 95th percentile skew surge and maxima, over the three time slices.

Projected changes in skew surge return periods are shown in Figure 5b, which give an indication of the magnitude of baseline, near future, and far future storm events up to a 1/50-year return period. The shaded area shows variability in return periods across the 12 ensembles, and solid lines show ensemble mean. The magnitude of a mean 1/20-year skew surge shifts from 0.71 m under baseline conditions to 0.74 m in the far future time slice (a 4% increase). The magnitude of a mean 1/50-year skew surge shifts from 0.79 m under baseline conditions to 0.82 m in far future time slice (a 3.8% increase). The range of skew surge magnitude across far future simulations

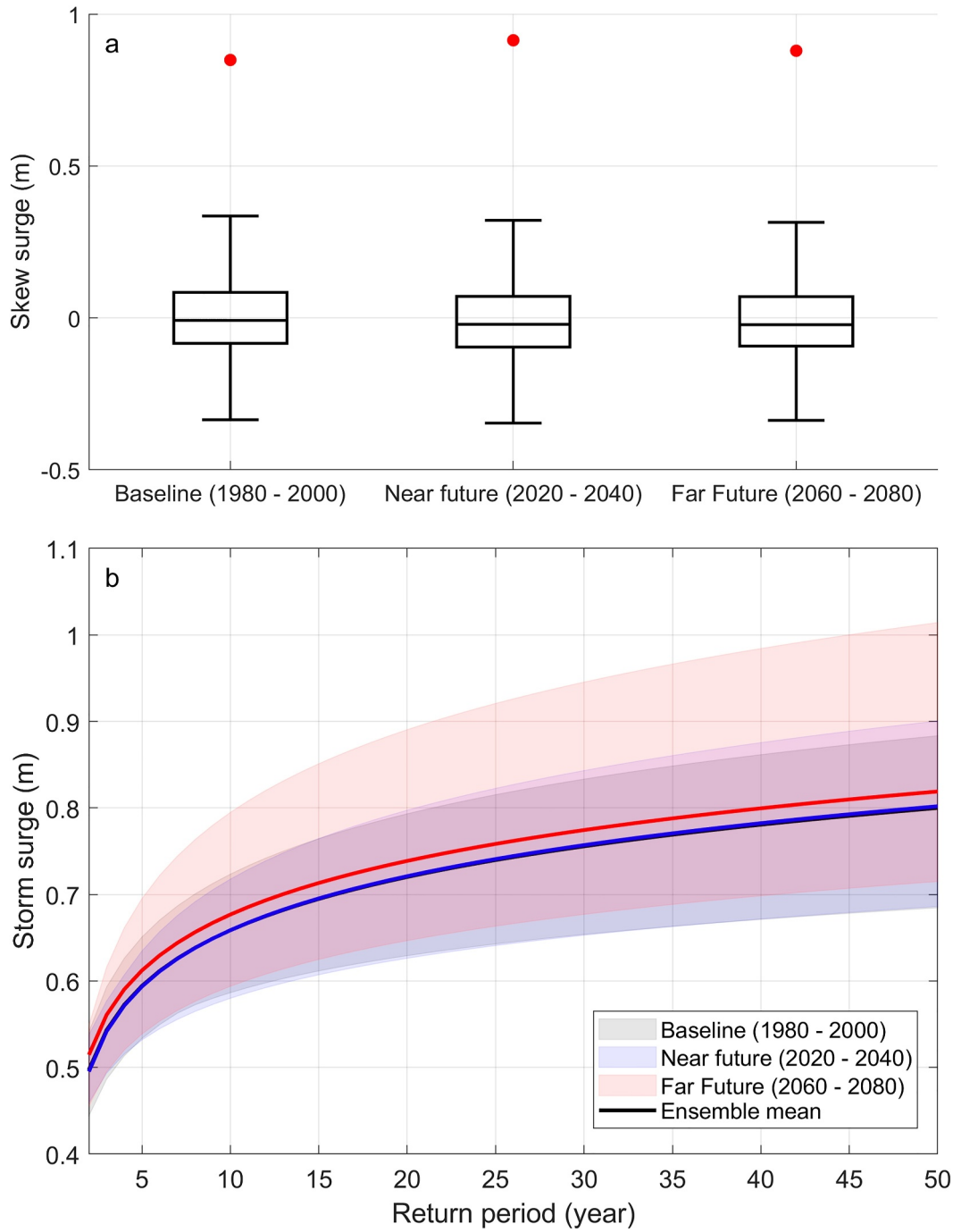

Figure 5. (a) Interquartile range (box), whiskers indicating furthest data point within the 1.5 * Interquartile range from the quartiles (vertical lines), median (center black line), mean (cross), maximum outlier (red dot) averaged across 12 perturbed parameter ensemble (PPEs) for baseline, near and far future skew surge projections; (b) Skew surge return periods for the baseline, near and far future simulations. Shaded areas shows uncertainty across bootstrapped data for 12 PPEs, and solid line shows ensemble mean. Figure S6 in Supporting Information S1 shows result for each PPE.

is noticeably wider than for near future, and baseline shows the narrowest range. The upward shift in skew surge magnitude indicates that (a) a 0.5 cm skew surge, as an example, will have a lower return period; or (b) a 1/10-year return period skew surge will be a higher magnitude.

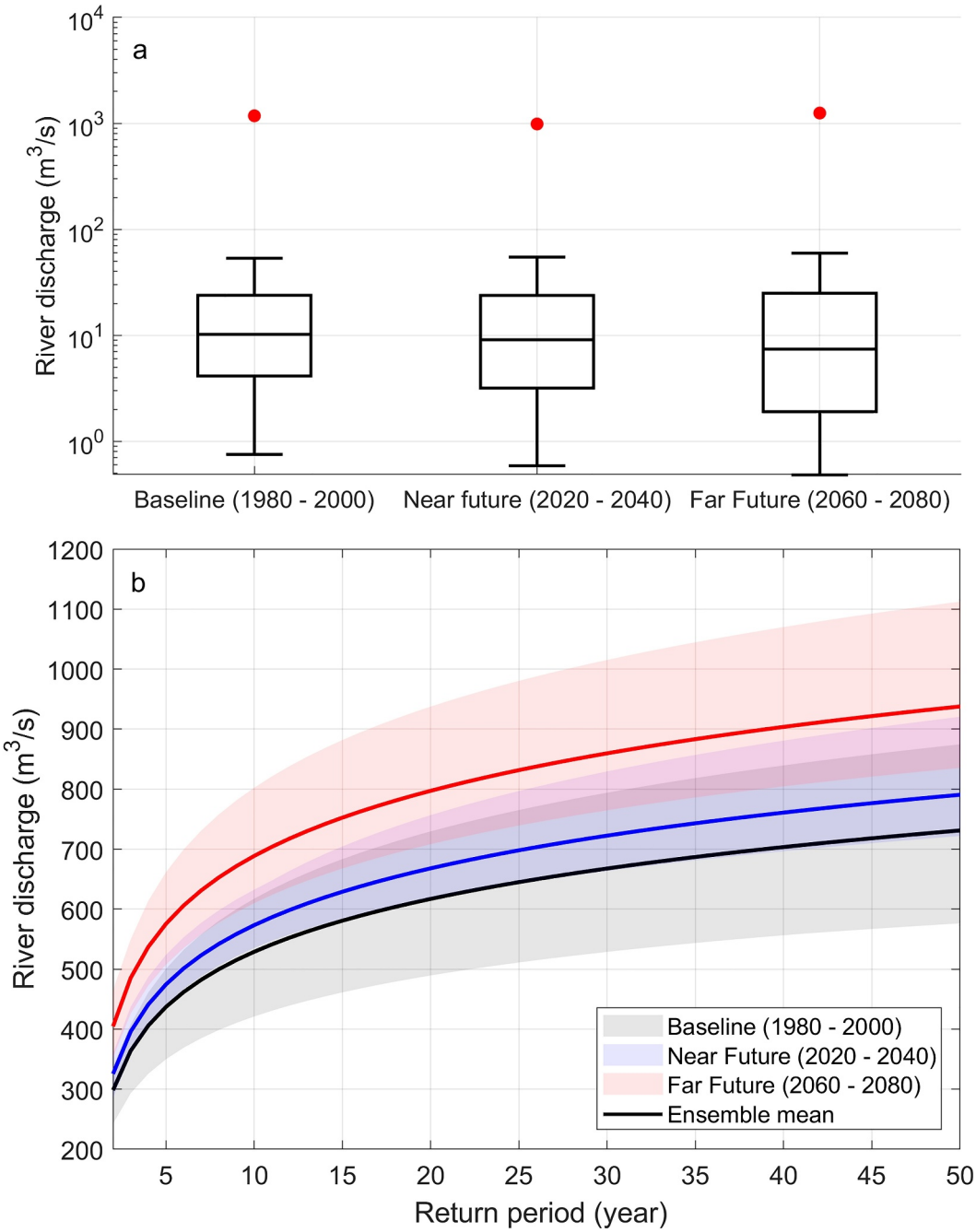

Figure 6. (a) Interquartile range (box), whiskers indicating furthest data point within the 1.5 * Interquartile range from the quartiles (vertical lines), median (center black line), mean (cross), maximum outlier (red dot) averaged first across 100 hydrology runs and then across 12 perturbed parameter ensemble members (PPEs) for baseline, near and far future river discharge projections. See Figure S9 in Supporting Information S1 for percentiles on a linear *y*-axis (b) projected peak river discharge return periods for baseline, near and far future time slices. Shaded area shows uncertainty across all 100 hydrology runs and 12 PPEs and solid line shows ensemble mean. Figure S10 in Supporting Information S1 shows result for each PPE.

3.2. Future Changes in River Discharge

Projected changes in the magnitudes of peak river discharges are shown in Figure 6a, between projected baseline, near future, and far future scenarios. Means, quantiles, and outliers were calculated for each of the 100 best performing hydrological runs (Figures S7 and S8 in Supporting Information S1) then presented across the 12 ensemble members, and across each time slice. The projected median discharge shows a decrease from 10.2 m^3/s

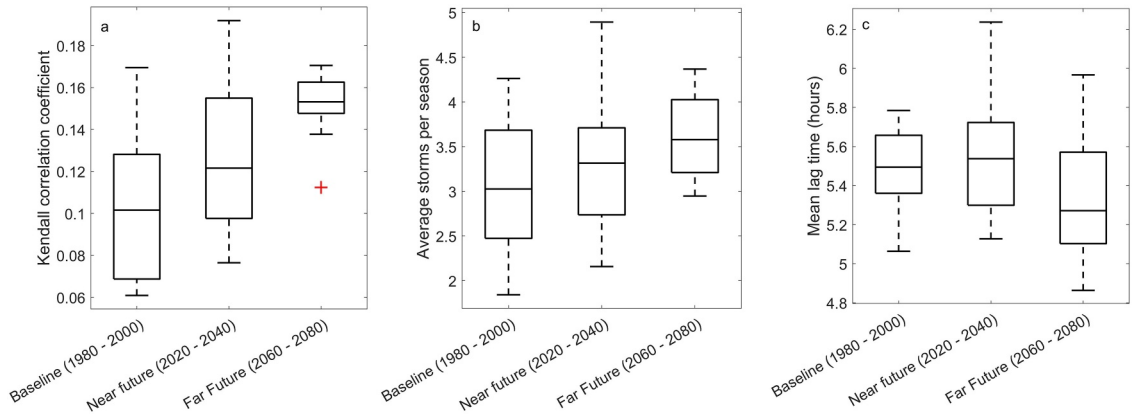

Figure 7. Projected changes for (a) Kendall rank correlation coefficient between peak river discharge and associated skew surge; (b) Mean number of extreme compound events (both drivers >95th percentile) per season (May–June); (c) Mean time lag (hours) between peak skew surge and peak discharge (both drivers >95th percentile). Data is shown as interquartile ranges (boxes), with whiskers indicating furthest data point within the 1.5 * interquartile range from the quartiles (vertical lines), median (center black line), maximum outlier (red cross) averaged across 12 perturbed parameter ensemble members (PPEs) for baseline, near and far future time slices. See Figure S11 in Supporting Information S1 for results for individual PPEs.

in baseline, to 7.4 m^3/s in far future time slices (−27%). However, the 75th and 95th percentile discharge show a noticeable increase in magnitude from near future to far future: for the 75th percentile, from 80.3 m^3/s to 100 m^3/s (+24.5%); and for the 95th percentile, from 128.46 m^3/s to 168 m^3/s (+30.8%). The (maximum) outliers (red circles, Figure 6) are shown to decrease from baseline to near future, and then increase, exceeding 1,250 m^3/s in far future.

Projected changes of peak river discharge return periods, for the baseline, near future, and far future time slice are shown for up to 1/50-year return periods (Figure 6b). Solid lines show the ensemble mean return periods, and the shaded area shows the range across the 12 ensemble members. The magnitude of discharge associated with each return period will increase up to 2080. While mean river discharge shows a slight decline over time (Figure 6a), the return level curves in Figure 6b reflect changes in annual maximum discharge. These extremes increase in magnitude resulting in an upward shift in return levels. A 1/20-year event will generate a baseline discharge of 617 m^3/s, near future of 668 m^3/s, and far future of 797 m^3/s, which is a 29% increase. A 1/50-year event will generate a baseline river discharge of 731 m^3/s, near future of 790 m^3/s, and far future of 937 m^3/s, which is a 28% increase. As seen for skew surge, the upward shift in river discharge magnitude indicates that (a) a 600 m^3/s discharge, as an example, will have a lower return period changing from a 1/17-year event under baseline conditions to a 1/6-year event; or (b) a 1/10-year return period discharge will be larger changing from representing 520 m^3/s under baseline conditions up to 692 m^3/s in far future.

3.3. Future Changes in Co-Occurrences

Projected changes in characteristics of the co-occurrences between skew surge and river discharge are shown in Figure 7. Previous research on storm driven compound events at the Dyfi estuary (using historic gauge data: 1984–2014) has shown a Kendall rank correlation coefficient of 0.25 between peaks in skew surge and river discharge, with an average of five extreme compound events per storm season (May-June), and an average 5-hr time lag between peaks (Lyddon et al., 2024).

Table 4
Estimates of Chi $\chi(u)$ for u Associated With a Range of Percentiles

	0.1	0.2	0.3	0.4	0.5	0.6	0.7	0.8	0.9	0.95	0.99
Baseline	0.91	0.82	0.71	0.61	0.52	0.41	0.26	0.17	0.08	0.03	0.02
Near future	0.91	0.81	0.71	0.6	0.51	0.41	0.29	0.19	0.1	0.04	0.03
Far future	0.91	0.82	0.71	0.61	0.52	0.43	0.34	0.24	0.13	0.07	0.06

10.1029/2024EF005822

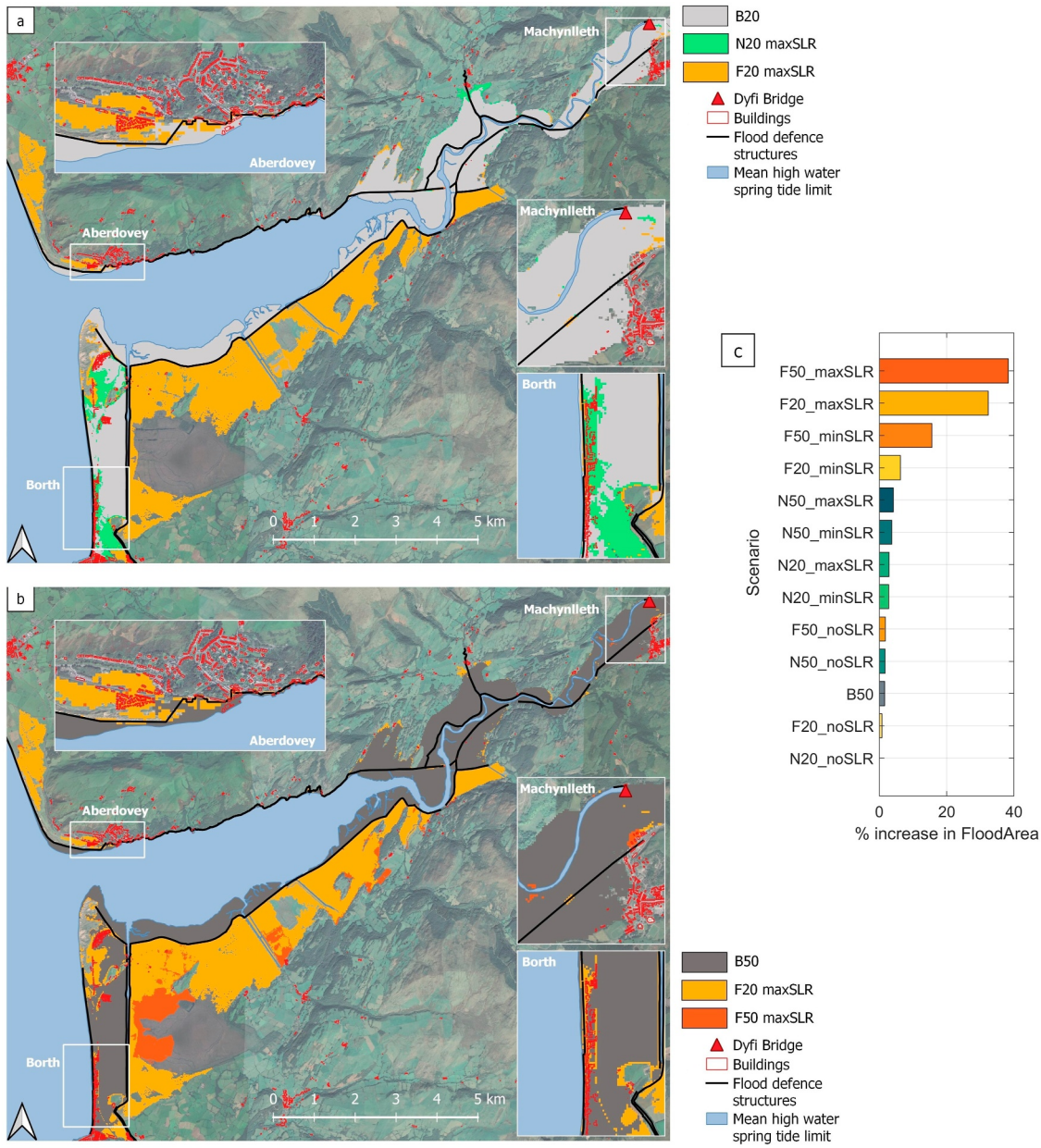

Figure 8. Simulated flood inundation maps for modeled compound event scenarios (simulations with smaller flood extent have been superimposed upon simulations with larger flood extent) which represent a range of storylines including (a) Far future 1/50-year event with different sea level rise (SLR); (b) Near and far future 1/20-year event with maximum SLR. Basemap and buildings © OpenStreetMap contributors 2023. Distributed under the Open Data Commons Open Database License (ODbL) v1.0. Flood defense structures distributed under Open Government License (NRW, 2020). (c) Increase in inundation extent (%) relative to the Baseline 1/20-year scenario (B20). The colors refer to scenarios in Table 3: blue/green indicate near-future scenarios; orange/red indicate far-future scenarios. Darker color indicates a higher return period and greater magnitude of SLR.

Figure 7a presents the Kendall rank correlation coefficient between pairs of skew surge and river discharge data, for the baseline, near future, and far future time slices. Mean correlations show an increasing but still weak overall relationship for baseline (0.10), near future (0.12), and far future (0.16) time slices. Further, the range of correlations across the 12 ensembles is narrower in the far future than earlier time slices. These projected correlations are weaker compared with the analyses of historical observational data. Figure 7b displays the mean number of storms per season (May–June) and Figure 7c shows the average time lag between peak skew surge and peak discharge. The frequency of extreme compound events occurring together is projected to increase on average from 3 (baseline) to 3.57 (far future), although there is considerable variability across the PPEs. Time lags

between peak skew surge and peak discharge are similar between the baseline and near future time slices, with a reduction of up to 1 hr projected for the far future time slice (Figure 7c). This indicates that peaks in both drivers will occur closer together in time, potentially amplifying the effects of compound flooding further.

3.4. Multi-Variance Extreme Value Analysis

Table 4 shows the estimates of χ for different percentiles, averaged across the 12 ensembles. The estimated value of $\chi(u)$ for u associated with the 90th percentile for the baseline (1980–2000) is 0.08. This value is close to zero, which indicates it is unlikely that the 90th percentile of most extreme compound events will occur concurrently. It is more likely that the 10th percentile of the most extreme compound events will occur concurrently ($\chi = 0.91$). There is little variation in dependence $\chi(u)$ between the most extreme compound events for baseline, near future, and far future time slices, for different given percentile thresholds. Tail dependence is shown to be marginally stronger under the most extreme percentile in the far future, compared to baseline and near future. Dependence in the far future is marginally stronger for the more extreme events from 70th to 99th percentile, with an increase in χ of 0.02–0.06.

3.5. Inundation Modeling of Projected Future Compound Flooding

Model simulations of climate change induced compound flooding in the Dyfi estuary were performed for 14 scenarios (Table 2) using the LISFLOOD-FP hydrodynamic model (described in Section 2.5.2). Scenarios represent 1/20- and 1/50-year return period storm surge and river discharge conditions for baseline, near future, and far future conditions, with/without SLR representing mean RCP2.6 and RCP8.5 values.

Flood maps compare inundation extent for the two most extreme scenarios (Figure 8a), and difference between near- and far-future scenarios (Figure 8b). All flood maps are presented individually in Supplementary Information (Figure S12–S25 in Supporting Information S1). We show that the coastal village of Borth is exposed to flooding (from the estuary rather than coast), even with a present day 1/20-year compound event (B20, Figure 8). However, simulated flooding inundated presently populated areas (based on Open Street Map data) for near future and far future scenarios. The town of Aberdyfi (population = 682), for example, was simulated to be flooded for far future scenarios, while the town of Machynlleth (population = 2163) was largely not flooded (except to the north where the old Bridge). The simulations are only a snapshot of potential flooding scenarios and do not consider variability in driver behavior and timings, nor antecedent conditions. Further, these simulations do not consider future potential changes in land use, land management, urbanization, and flood defences.

Figure 8c shows projected percentage change in flood extent across the Dyfi model domain for each scenario, relative to the baseline 1/20-year scenario (B20). Most percentage change in flood extent occurs under the far future scenarios, especially with increases in SLR included, generating up to 38% more inundation extent from the present-day 1/20-year scenario. Results for the near future scenarios differ in that the return period (1/20-year or 1/50-year) is the primary driver of flood extent, rather than SLR. However, these percentage changes are smaller (<3%) between near future scenarios (green bars on Figure 8).

4. Discussion

This research presents the first use of high spatio-temporal resolution, physically consistent, 21st century climate projections of marine and fluvial behavior that have been used together to assess potential changes in extreme storm-driven compound events and flooding in a case study estuary. Focusing on the Dyfi Estuary, west-UK, and considering 12 PPEs from a high emissions future (RCP8.5; see Devitt, 2023; Tinker et al., 2024), we show that: (a) peak river discharge magnitudes and return periods are expected to increase (Figure 5), while skew surges will show little change (Figure 6); (b) compound events will become more likely, more frequent, and more in-phase (Figure 7); and (c) these projected changes together with SLR projections will likely lead to increased flood inundation this century (up to +36%) (Figure 8). In the near future, flood inundation was sensitive to the severity of the drivers (e.g., 1/20-year vs. 1/50-year compound events), although toward the end of the century SLR projections dominate the flood hazard. As similar climate data becomes available for other estuaries nationally and worldwide, it will be important to understand how our findings for the Dyfi translate to a general climate impact storyline.

From our analyses, annual mean skew surge values are projected to increase only marginally into the far future (2060–2080), by ∼3 cm, and showed little change by the near future (2020–2040) (Figure 6a). The bootstrap resampling of annual maxima methodology used here, based on 12 PPEs and where one ensemble exhibited distinctly more extreme skew surge values than the others, could have influenced the resampled outcomes. However, since it is computationally expensive to run additional climate simulations at hourly and sub-mesoscale resolutions (to a similar ensemble number as done by Tinker et al., 2024), methods are continuing to be developed to use these climate projections as robustly as possible (Chan et al., 2023; Holt et al., 2025). Analysis of 21st Century projected changes in storm surge climate for the UK, derived directly from coarser RCMs or GCMs, are of the same order as the natural climatological variability (Howard et al., 2010; Woth et al., 2005) and emphasize the dominance of changes in time-mean sea level in driving changes in future coastal sea level extremes and flood hazard (e.g., Cannaby et al., 2016; Howard et al., 2014; Lowe et al., 2010). A subset of the Climate Model Intercomparison Project Phase 5 (CMIP5, Taylor et al., 2012) simulations were used to explore UK coastal skew surge trends and concluded that there is no evidence for significant changes in future storm surges in the UK (Palmer et al., 2018). We show no significant future changes in surge values in the Dyfi estuary, but estuarine resonance, wave setup, river inflow, and tidal phase effects can create a distinct local surge response highlighting the importance of site-specific surge assessments. It has been shown that SLR will likely change the frequency of extreme sea level events (Kirezci et al., 2020; Tebaldi et al., 2021; Vousdoukas et al., 2018). Future research incorporating both projected SLR with total water level (tide + surge) would provide additional insight on future extreme sea level hazard for risk assessment and adaptation planning at this and other sites.

Our analysis of projections of river discharge indicates more substantial changes; for example, with increases into the far future of up to 180 m^3/s (29%) for a 1/20-year return period and 206 m^3/s (75%) for a 1/50-year return period (Figure 7b). We show that mean discharge is also likely to increase into the near and far future, with broader distributions and longer tails to the extremes (Figure 7a). This suggests that extreme river flows are becoming more prominent in the Dyfi. Extreme discharge is driven by extreme rainfall behavior; indeed, several studies using global observation data have suggested that precipitation events have intensified in the last 30–50 years (Fischer & Knutti, 2016; Gundmussen et al., 2021; Westra et al., 2013), and using GCM have shown the magnitude of rainfall extremes will intensify further this century (Chan et al., 2023; Fowler & Kilsby, 2007; Fowler, Ali, et al., 2021; Fowler, Lendernik, et al., 2021). Whilst these projected changes in precipitation can be used as a proxy for changes in river discharge, the coarse scales do not account for spatial distribution in rainfall at catchment-scale nor variability in land use (Ranasinghe et al., 2021). Future assessments of potential changes in UK river flows, using UKCP18 12 km RCM PPEs and a national-scale Grid-to-Grid hydrological model, showed potential increases in winter mean and high flows, and in summer decreases in mean and low flows, albeit with wide uncertainty ranges (Kay, 2021, 2022).

Our analyses of future changes in storm surges and river discharges aligns well with the literature; but further to this, our study—using higher spatio-temporal data resolution data than previous studies—highlights the need to predict not only potential changes in the magnitude of extremes in these drivers but also their joint dependence, joint probability, relative timings, and how these changes are likely to lead on to flood hazard into the future. We show that the characteristics and behavior of storm-driven compound flood events are projected to change this century (Figure 7). Although marine and fluvial extremes remain largely independent in the upper tail, the increasing χ values (from 0.02 to 0.06) suggest a modest rise in the likelihood of joint extremes. This suggests a higher likelihood of extreme peak flows coinciding with extreme storm surges and a potential increase in dependence under future scenarios. The mean frequency of events where both drivers exceed the 95th percentile is rising from 3 to 3.6 per year, and the increase in tail dependence points to a stronger correlation between extreme marine and fluvial values, further amplifying the risk of compound flooding. Additionally, the time lag between these peaks is shortening by over an hour. Shorter time lags could be due to flashier hydrographs; as rainfall events become more intense peak discharge is reached quicker (Lane & Kay, 2021; Merz et al., 2021; Tabari, 2020). This quickening hydrological response increases the likelihood that high discharge will coincide with the storm surge driven by the same storm system. For the Dyfi, there is an increasing chance that both peak events will occur simultaneously, and this overlap can lead to more severe compound flooding (Harrison et al., 2021). The time lag that leads to the most severe compound flooding will likely depend on subtle changes in the behavior of the individual drivers and the specific location within the estuary being considered. This relationship is highly sensitive to the estuary's unique length, shape, and geometry.

Knowledge of the joint dependence of fluvial and marine drivers of estuarine flooding is essential for accurately predicting future flood probability, especially under the influence of climate change (Bevacqua et al., 2020; Ghanbari et al., 2021). It allows for a more comprehensive understanding of the risks, leading to better protection of infrastructure, ecosystems, and human communities (Kirkpatrick & Olbert, 2020; Lopes et al., 2022; Zellou & Rahali, 2019). The assumption of independence between events (e.g., assuming storm surges and river floods occur independently) could lead to underestimation of the true flood risk. Ignoring this joint dependence could result in underestimating the risk, leading to inadequate preparation and potentially devastating consequences for estuarine communities.

Direct comparison of upper tail dependence with previous studies is challenging due to differing methodologies, thresholds, and event definitions. However, the literature generally supports the finding of weak upper tail dependence between skew surge and river discharge. For example, Paprotny et al. (2020) identified surge events using a 90th percentile threshold of daily maxima surge and discharge, and aggregated consecutive days above this threshold. They then computed the maximum river discharge and precipitation during these storm windows. The resulting upper tail dependence coefficient, read from their Figure 1b, was approximately 0.25, indicating modest dependence. They do not calculate lower tail dependence.

Other studies using statistical thresholds to assess co-occurrence show weaker dependence. When assessing dependence on the upper 10% of skew surge events across south and west Britain, χ values estimated for river gauges nearby the Dyfi Estuary in Wales were consistently low (e.g., Glaslyn: 0.06; Leri: 0.03; Ystwyth: 0.04; Teifi: 0.13) (Svensson & Jones, 2004). This suggests very weak or negligible extremal dependence at the 90th percentile threshold. They do not calculate lower tail dependence. It is also worth noting that the dependence between river flow and sea surge can vary considerably across short distances, reflecting catchment-specific hydrological characteristics such as size, topography, and geology.

In our study, storm surge is modeled using the NEMO CO9 model, which directly includes tidal processes and the inverse barometer effect. We identify compound events based on the assumption that in the GCM and downscaled regional simulations, a low-pressure storm system simultaneously contributes to elevated fluvial and coastal water levels by producing precipitation (driving high discharge) and depressing atmospheric pressure (raising sea level). These events are paired when their respective peaks occur within a set time window. This set time window is based on observation data from the Dyfi Estuary, 20.42 hr.

However, the co-occurrence of discharge and surge peaks might not fully replicate observational reality. The sensitivity of compound event detection to this time lag has been noted in previous work (Green et al., 2025; Wahl et al., 2015), and we acknowledge that the optimal lag may differ between observations and the model. This may contribute to a weak tail dependence as extreme compound events may not identified within this set window.

Future research could explore the sensitivity of dependence metrics to the chosen time lag and consider the use of high-resolution, coastal climate models to better capture surge dynamics and compound event timing.

Through inundation modeling, we show how projected changes in sea level and river discharge extremes in the Dyfi estuary are likely influence flooding depth and extent (Figure 8). We show up to 40% more inundation area into the far future, considering a high-emissions future (RCP8.5) and "worst-case" scenario (1/50-year events). Our simulations, whilst not exhaustive in exploring how changing driver behaviors will alter the flood hazard, show that SLR will be a dominant driver of future coastal flood hazard alongside peak river flows. Compound flooding is not only sensitive to driver behavior but also to estuary shape, implying that our findings are indeed case sensitive to the Dyfi. However, the Dyfi is predominantly steep sided—other estuaries with larger floodplains are likely to experience increased changes in inundation area by similar patterns of driver changes due to greater space for floodwater. One case study was used here due to constraints on data availability, but the research can be expanded to other estuaries to explore transferability in the future when new sub-daily hydrological projections become available. Previous research in the Severn estuary has shown that just a 6 cm increase in coastal water level (combined tide, surge, and wave) can substantially increase flood inundation by 19%, and suburban damage costs by 25% (Lyddon et al., 2020), highlighting the vulnerability of low-lying estuary communities to such changes. Rising sea levels can reduce the capacity of estuaries to drain riverine floodwaters, as well as increase river levels several kilometres upstream, that is, SLR will reshape and shift the estuary landward. Hence, SLR could reduce the effectiveness of levees or flood defences.

To effectively assess and understand changes in compound flooding risks, sea level and river discharge projections must be derived from the same GCM, using the same ensemble members, for the same time period, and at the same temporal resolution. We used only a high-emissions future (RCP8.5) in our study (although also included a low-emissions (RCP2.6) SLR scenario). Incorporating a range of possible futures and using different GCMs would offer a more comprehensive understanding of potential future changes, as this data becomes available. It is necessary to use climate projections with good temporal resolution (e.g., hourly, or sub-daily, for resolving hydrological extremes in smaller catchments such as the majority in the UK and Europe). It is also preferable to use continuous projections extending up to 2100 to best capture trends in climatology. Projecting sub-daily river discharges under climate change is difficult due to the need for high temporal and spatial resolution precipitation data, and the uncertainties inherent in climate and hydrological models. The use of CPMs is helping to develop this understanding (Kendon et al., 2017). However, running models that simulate hydrological processes at sub-daily intervals over long periods (e.g., multiple decades) is computationally expensive (Fowler, Ali, et al., 2021). GCMs and RCMs do not currently resolve coastal and estuarine bathymetries well for estuarine impact assessments (Tinker et al., 2024). Further downscaling to coastal inundation models are often needed to correctly resolve water level extremes propagating into estuaries. Additionally, coastal, estuarine, and riverine bathymetries are often poorly resolved and require further surveys (Prampolini et al., 2020; Robins et al., 2016, 2018). Cascading downscaled marine and fluvial projections to a hydrodynamic, estuary impact model is a novel development in hazard assessment here, and additional characteristics of storm-driven compound flooding could be modelled, including changes in time lag, storm surge shape, and storm clustering. Our exemplar study for the Dyfi estuary requires upscaling nationally, as suitable climate projections become available, which can then be applied to other regions where such projections become available.

Neither marine nor fluvial projections currently account for potential changes to estuarine morphology (e.g., sediment loading, erosion, accretion), wave behavior (e.g., significant wave height, wave period), ecosystem dynamics (e.g., productivity, biomass, chlorophyll), or water quality (e.g., nutrient levels, oxygen levels, pollution). Sea-level rise is expected to alter geomorphic and hydro-ecologic feedback loops in estuaries, and likely to cause estuarine shoreline retreat, infilling, sediment redistribution, and altered tidal dynamics (Khojasteh et al., 2021; Weisscher et al., 2023). Also, future changes in land use and urbanisation in estuaries will be important as this will change the physical routing of catchment drainage (e.g., runoff and groundwater dynamics, as well as water quality), and in turn affect the vulnerability and exposure of communities. Urbanisation can increase impermeable surfaces, and influence hydrological behavior dependent on surface type, age and condition (Redfern et al., 2016). A return period of 1/100-year may be doubled in size by a 30% paving of the basin (Hollis, 1975) as roads, roofs and pavements reduce infiltration and increases surface runoff, therefore potentially leading to quicker river response to rainfall (Chen et al., 2017). In further studies, it would be interesting to investigate to what extent anthropogenic activities will further alter climate-driven changes in compound flooding.

5. Conclusion

We present the first analysis of combined coastal sea level and fluvial projections, downscaled to hourly and sub-mesoscales, to assess future changes in storm-driven compound flooding, with a focus on the Dyfi Estuary, west UK. By employing physically consistent projections of a high emissions future (RCP8.5, 12 perturbed parameter ensembles), analyzed for three time slices (1980–2000, 2020–2040, 2060–2080), we independently evaluated changes in both coastal sea level and river discharge drivers and examined their interdependence. Based on the ensemble mean, our findings indicated small changes in storm surge magnitude but provided evidence for more extreme peak river flows in the future. Importantly, we observed changes in the behavior of these drivers when considered together, such as increasing dependence (i.e., extreme river discharge will more likely occur at same time as extreme sea level), increasing co-occurrence (i.e., combined surge and discharge extremes will occur more often per year), decreasing time lag between peaks in sea level and river discharge (to potentially amplify the effects of compound flooding), and increasing extreme tail dependence (Table 4). By applying these projections to an estuary inundation model, we demonstrate that a relatively "worst-case" storm such as a 1/50-year event will increase flood inundation up to 40% by 2080. These results underscore the necessity of incorporating joint probability and dependence between marine and fluvial drivers in flood hazard assessments. By combining hourly projections of river discharge with hourly projections of SSH and residual surge, this method offers a scalable approach that can be applied globally wherever such projections exist (driven by the same GCM). Extending

projections in time beyond 2100 would support long-term flood planning, but requires consideration of model uncertainties, evolving climate scenarios, socioeconomic changes, and long-term adaptation measures (Easterling et al., 2024; Heslop et al., 2024). The study highlights the critical need for physically consistent and appropriately downscaled marine and fluvial projections to accurately simulate and predict future flood hazards, emphasizing the importance of a comprehensive approach to understanding compound flooding under changing climatic conditions.

Conflict of Interest

The authors declare no conflicts of interest relevant to this study.

Data Availability Statement

The NWSPPE data sets are available via CEDA (https://catalogue.ceda.ac.uk/uuid/832677618370457f9e0a85da021c1312, Tinker, 2023). User registration is required. UKCP Local data are alternatively available via the UKCP data portal at https://ukclimateprojections-ui.metoffice.gov.uk/ (Met Office Hadley Centre, 2018). User registration is required. Observation tide gauge data is available from National Tidal and Sea Level Facility (https://www.bodc.ac.uk/data/hosted_data_systems/sea_level/uk_tide_gauge_network/processed/). Select Barmouth or Fishguard tide gauge for records. User registration is required. Further details of Barmouth tide gauge site are available at https://ntslf.org/tides/uk-network/portinfo?port=Barmouth. Observation river gauge data is available from National River Flow Archive (NRFA) (https://nrfa.ceh.ac.uk/data/search). Data for Dyfi Bridge (gauge ID 64001) is available at https://nrfa.ceh.ac.uk/data/station/info/64001.

Acknowledgments
This research has been supported by the Natural Environment Research Council (NE/V004239/1). Jonathan Tinker was supported by the Met Office Hadley Centre Climate Programme funded by DSIT and Defra. Laura Devitt was supported by the Water Informatics: Science and Engineering (WISE) Centre for Doctoral Training (CDT). Gemma Coxon was supported by a UKRI Future Leaders Fellowship (MR/V022857/1). Both Laura Devitt and Gemma Coxon were supported by FUTURE-FLOOD (NE/X014134/1).

References

Alifu, H., Hirabayashi, Y., Imada, Y., & Shiogama, H. (2022). Enhancement of river flooding due to global warming. *Scientific Reports*, *12*(1), 20687. https://doi.org/10.1038/s41598-022-25182-6

Archer, L., Hatchard, S., Devitt, L., Neal, J. C., Coxon, G., Bates, P. D., et al. (2024). Future change in urban flooding using new convection-permitting climate projections. *Water Resources Research*, *60*(1), e2023WR035533. https://doi.org/10.1029/2023wr035533

Barada, M., Robins, P., Lewis, M., & Skov, M. (2022). The importance of estuary shape in evaluating the flood risk in estuaries, EGU General Assembly 2022, Vienna, Austria, 23–27 May 2022, EGU22-4086. https://doi.org/10.5194/egusphere-egu22-4086

Bates, P. D., Horritt, M. S., & Fewtrell, T. J. (2010). A simple inertial formulation of the shallow water equations for efficient two-dimensional flood inundation modelling. *Journal of Hydrology*, *387*(1–2), 33–45. https://doi.org/10.1016/j.jhydrol.2010.03.027

Bates, P. D., Quinn, N., Sampson, C., Smith, A., Wing, O., Sosa, J., et al. (2021). Combined modeling of US fluvial, pluvial, and coastal flood hazard under current and future climates. *Water Resources Research*, *57*(2), e2020WR028673. https://doi.org/10.1029/2020WR028673

Batstone, C., Lawless, M., Tawn, J., Horsburgh, K., Blackman, D., McMillan, A., et al. (2013). A UK best-practice approach for extreme sea-level analysis along complex topographic coastlines. *Ocean Engineering*, *71*, 28–39. https://doi.org/10.1016/j.oceaneng.2013.02.003

Bevacqua, E., Maraun, D., Hobæk Haff, I., Widmann, M., & Vrac, M. (2017). Multivariate statistical modelling of compound events via pair-copula constructions: Analysis of floods in Ravenna (Italy). *Hydrology and Earth System Sciences*, *21*(6), 2701–2723. https://doi.org/10.5194/hess-21-2701-2017

Bevacqua, E., Maraun, D., Vousdoukas, M. I., Voukouvalas, E., Vrac, M., Mentaschi, L., & Widmann, M. (2019). Higher probability of compound flooding from precipitation and storm surge in Europe under anthropogenic climate change. *Science Advances*, *5*(9), eaaw5531. https://doi.org/10.1126/sciadv.aaw5531

Bevacqua, E., Vousdoukas, M. I., Zappa, G., Hodges, K., Shepherd, T. G., Maraun, D., et al. (2020). More meteorological events that drive compound coastal flooding are projected under climate change. *Communications Earth & Environment*, *1*(1), 47. https://doi.org/10.1038/s43247-020-00044-z

Camus, P., Haigh, I. D., Nasr, A. A., Wahl, T., Darby, S. E., & Nicholls, R. J. (2021). Regional analysis of multivariate compound coastal flooding potential around Europe and environs: Sensitivity analysis and spatial patterns. *Natural Hazards and Earth System Sciences*, *21*(7), 2021–2040. https://doi.org/10.5194/nhess-21-2021-2021

Cannaby, H., Palmer, M. D., Howard, T., Bricheno, L., Calvert, D., Krijnen, J., et al. (2016). Projected sea-level rise and changes in extreme storm surge and wave events during the 21st century in the region of Singapore. *Ocean Science*, *12*(3), 613–632. https://doi.org/10.5194/os-12-613-2016

Chan, S. C., Kendon, E. J., Berthou, S., Fosser, G., Lewis, E., & Fowler, H. J. (2020). Europe-wide precipitation projections at convection permitting scale with the unified model. *Climate Dynamics*, *55*(3–4), 409–428. https://doi.org/10.1007/s00382-020-05192-8

Chan, S. C., Kendon, E. J., Fowler, H. J., Blenkinsop, S., Roberts, N. M., & Ferro, C. A. T. (2014). The value of high-resolution met office regional climate models in the simulation of multihourly precipitation extremes. *Journal of Climate*, *27*(16), 6155–6174. https://doi.org/10.1175/JCLI-D-13-00723.1

Chan, S. C., Kendon, E. J., Fowler, H. J., Youngman, B. D., Dale, M., & Short, C. (2023). New extreme rainfall projections for improved climate resilience of urban drainage systems. *Climate Services*, *30*, 100375. https://doi.org/10.1016/j.cliser.2023.100375

Chen, J., Theller, L., Gitau, M. W., Engel, B. A., & Harbor, J. M. (2017). Urbanization impacts on surface runoff of the contiguous United States. *Journal of Environmental Management*, *187*, 470–481. https://doi.org/10.1016/j.jenvman.2016.11.017

Chen, Z., Zhou, T., Zhang, L., Chen, X., Zhang, W., & Jiang, J. (2020). Global land monsoon precipitation changes in CMIP6 projections. *Geophysical Research Letters*, *47*(14), e2019GL086902. https://doi.org/10.1029/2019gl086902

Church, J. A., Clark, P. U., Cazenave, A., Gregory, J. M., Jevrejeva, S., Levermann, A., et al. (2013). Sea-level rise by 2100. *Science*, *342*(6165), 1445. https://doi.org/10.1126/science.342.6165.1445-a

Coles, S., Heffernan, J., & Tawn, J. (1999). Dependence measures for extreme value analyses. *Extremes*, *2*(4), 339–365. https://doi.org/10.1023/a:1009963131610

Couasnon, A., Eilander, D., Muis, S., Veldkamp, T. I. E., Haigh, I. D., Wahl, T., et al. (2020). Measuring compound flood potential from river discharge and storm surge extremes at the global scale. *Natural Hazards and Earth System Sciences*, *20*(2), 489–504. https://doi.org/10.5194/nhess-20-489-2020

Coulthard, T. J., Neal, J. C., Bates, P. D., Ramirez, J., de Almeida, G. A. M., & Hancock, G. R. (2013). Integrating the LISFLOOD-FP 2D hydrodynamic model with the CAESAR model: Implications for modelling landscape evolution. *Earth Surface Processes and Landforms*, *38*(15), 1897–1906. https://doi.org/10.1002/esp.3478

Coxon, G., Freer, J., Lane, R., Dunne, T., Knoben, W. J. M., Howden, N. J. K., et al. (2019). DECIPHeR v1: Dynamic fluxEs and connectivity for predictions of HydRology. *Geoscientific Model Development*, *12*(6), 2285–2306. https://doi.org/10.5194/gmd-12-2285-2019

Defra / Environment Agency. (2005). *Joint probability: Dependence mapping and best practice: Technical report on dependence mapping*. Defra / Environment Agency R&D FD2308/TR1.

Devitt, L. (2023). *Estimating flood risk under climate change. PhD thesis*. University of Bristol. Retrieved from https://research-information.bris.ac.uk/en/studentTheses/estimating-flood-risk-under-climate-change

Easterling, D. R., Kunkel, K. E., Crimmins, A. R., & Wehner, M. F. (2024). Long-term planning requires climate projections beyond 2100. *Nature Climate Change*, *14*(9), 887–888. https://doi.org/10.1038/s41558-024-02085-0

Emanuel, K. (2017). Assessing the present and future probability of hurricane Harvey's rainfall. *Proceedings of the National Academy of Sciences*, *114*(48), 12681–12684. https://doi.org/10.1073/pnas.1716222114

Environment Agency. (2018). *Coastal design sea levels – Coastal flood boundary surge shape data 2018*. Environment Agency. Retrieved from https://environment.data.gov.uk/dataset/84c97c5e-d465-11e4-afbd-f0def148f590

Ferranti, E., Chapman, L., & Whyatt, D. (2017). A perfect storm? The collapse of Lancaster's critical infrastructure networks following intense rainfall on 4/5 December 2015. *Weather*, *72*(1), 3–7. https://doi.org/10.1002/wea.2907

Feyen, L., Dankers, R., Bódis, K., Salamon, P., & Barredo, J. I. (2011). Fluvial flood risk in Europe in present and future climates. *Climatic Change*, *112*(1), 47–62. https://doi.org/10.1007/s10584-011-0339-7

Fischer, E. M., & Knutti, R. (2016). Observed heavy precipitation increase confirms theory and early models. *Nature Climate Change*, *6*(11), 986–991. https://doi.org/10.1038/nclimate3110

Fosser, G., Gaetani, M., Kendon, E. J., Adinolfi, M., Ban, N., Belušić, D., et al. (2024). Convection-permitting climate models offer more certain extreme rainfall projections. *Climate and Atmospheric Science*, *7*(1), 51. https://doi.org/10.1038/s41612-024-00600-w

Fowler, H. J., Ali, H., Allan, R. P., Ban, N., Barbero, R., Berg, P., et al. (2021a). Towards advancing scientific knowledge of climate change impacts on short-duration rainfall extremes. *Philosophical Transactions of the Royal Society A: Mathematical, Physical and Engineering Sciences*, *379*(2195), 20190542. https://doi.org/10.1098/rsta.2019.0542

Fowler, H. J., & Kilsby, C. G. (2007). Using regional climate model data to simulate historical and future river flows in northwest England. *Climatic Change*, *80*(3–4), 337–367. https://doi.org/10.1007/s10584-006-9117-3

Fowler, H. J., Lenderink, G., Prein, A. F., Westra, S., Allan, R. P., Ban, N., et al. (2021). Anthropogenic intensification of short-duration rainfall extremes. *Nature Reviews Earth & Environment*, *2*(2), 107–122. https://doi.org/10.1038/s43017-020-00128-6

Fritz, H. M., Blount, C. D., Thwin, S., Thu, M. K., & Chan, N. (2009). Cyclone Nargis storm surge in Myanmar. *Nature Geoscience*, *2*(7), 448–449. https://doi.org/10.1038/ngeo558

Ganguli, P., Paprotny, D., Hasan, M., Güntner, A., & Merz, B. (2020). Projected changes in compound flood hazard from riverine and coastal floods in Northwestern Europe. *Earth's Future*, *8*(11), e2020EF001752. https://doi.org/10.1029/2020ef001752

Ghanbari, M., Arabi, M., Kao, S., Obeysekera, J., & Sweet, W. (2021). Climate change and changes in compound coastal-riverine flooding hazard along the U.S. coasts. *Earth's Future*, *9*(5), e2021EF002055. https://doi.org/10.1029/2021ef002055

Green, J., Haigh, I. D., Quinn, N., Neal, J., Wahl, T., Wood, M., et al. (2025). Review article: A comprehensive review of compound flooding literature with a focus on coastal and estuarine regions. *Natural Hazards and Earth System Sciences*, *25*(2), 747–816. https://doi.org/10.5194/nhess-25-747-2025

Griffith, H. V., Wade, A. J., Lavers, D. A., & Watts, G. (2020). Atmospheric river orientation determines flood occurrence. *Hydrological Processes*, *34*(23), 4547–4555. https://doi.org/10.1002/hyp.13905

Gudmundsson, L., Boulange, J., Do, H. X., Gosling, S. N., Grillakis, M. G., Koutroulis, A. G., et al. (2021). Globally observed trends in mean and extreme river flow attributed to climate change. *Science*, *371*(6534), 1159–1162. https://doi.org/10.1126/science.aba3996

Gupta, H. V., Kling, H., Yilmaz, K. K., & Martinez, G. F. (2009). Decomposition of the mean squared error and NSE performance criteria: Implications for improving hydrological modelling. *Journal of Hydrology*, *377*(1–2), 80–91. https://doi.org/10.1016/j.jhydrol.2009.08.003

Haigh, I. D., Wadey, M. P., Wahl, T., Ozsoy, O., Nicholls, R. J., Brown, J. M., et al. (2016). Spatial and temporal analysis of extreme sea level and storm surge events around the coastline of the UK. *Scientific Data*, *3*(1), 160107. https://doi.org/10.1038/sdata.2016.107

Haigh, I. D., Wahl, T., Rohling, E. J., Price, R. M., Pattiaratchi, C. B., Calafat, F. M., & Dangendorf, S. (2014). Timescales for detecting a significant acceleration in sea-level rise. *Nature Communications*, *5*(1), 3635. https://doi.org/10.1038/ncomms4635

Hallegatte, S., Green, C., Nicholls, R. J., & Corfee-Morlot, J. (2013). Future flood losses in major coastal cities. *Nature Climate Change*, *3*(9), 802–806. https://doi.org/10.1038/nclimate1979

Harrison, L. M., Coulthard, T. J., Robins, P. E., & Lewis, M. J. (2021). Sensitivity of estuaries to compound flooding. *Estuaries and Coasts*, *45*(5), 1250–1269. https://doi.org/10.1007/s12237-021-00996-1

Hendry, A., Haigh, I. D., Nicholls, R. J., Winter, H., Neal, R., Wahl, T., et al. (2019). Assessing the characteristics and drivers of compound flooding events around the UK Coast. *Hydrology and Earth System Sciences*, *23*(7), 3117–3139. https://doi.org/10.5194/hess-23-3117-2019

Hermans, T. H. J., Tinker, J., Palmer, M. D., Katsman, C. A., Vermeersen, B. L. A., & Slangen, A. B. A. (2020). Improving sea-level projections on the Northwestern European shelf using dynamical downscaling. *Climate Dynamics*, *54*(3–4), 1987–2011. https://doi.org/10.1007/s00382-019-05104-5

Heslop, J., Nicholls, R., Ballesteros Martinez, C., Linke, D., & Hinkel, J. (2024). Global assessment of human exposure to sea-level rise to 2300. EGU General Assembly 2024, Vienna, Austria, 14–19 Apr 2024, EGU24-20522. https://doi.org/10.5194/egusphere-egu24-20522

Hoitimk, A. J. F., & Jay, D. A. (2016). Tidal river dynamics: Implications for deltas. *Reviews of Geophysics*. https://doi.org/10.1002/2015rg000507

Hollis, G. E. (1975). The effect of urbanization on floods of different recurrence interval. *Water Resources Research*, *11*(3), 431–435. https://doi.org/10.1029/wr011i003p00431

Holt, J., Katavouta, A., Hopkins, J., Amoudry, L. O., Appendini, C. M., Arneborg, L., et al. (2025). Future climate projections in the global coastal ocean. *Progress in Oceanography*, *235*, 103497. https://doi.org/10.1016/j.pocean.2025.103497

Howard, T., Lowe, J., & Horsburgh, K. (2010). Interpreting century-scale changes in Southern North Sea storm surge climate derived from coupled model simulations. *Journal of Climate*, *23*(23), 6234–6247. https://doi.org/10.1175/2010jcli3520.1

Howard, T., Palmer, M. D., Jackson, L. C., & Yamazaki, K. (2024). Storm surge changes around the UK under a weakened Atlantic meridional overturning circulation. *Environmental Research Communications*, *6*(3), 035026. https://doi.org/10.1088/2515-7620/ad3368

Howard, T., Pardaens, A. K., Bamber, J. L., Ridley, J., Spada, G., Hurkmans, R. T. W. L., et al. (2014). Sources of 21st century regional sea-level rise along the coast of northwest Europe. *Ocean Science*, *10*(3), 473–483. https://doi.org/10.5194/os-10-473-2014

IPCC. (2021). IPCC: Summary for policymakers (AR6). In V. Masson-Delmotte, P. Zhai, A. Pirani, S. L. Connors, C. Péan, et al. (Eds.), *Climate change 2021: The physical science basis. Contribution of working group I to the sixth assessment report of the intergovernmental panel on climate change* (pp. 3–32). Cambridge University Press. https://doi.org/10.1017/9781009157896.001

Jane, R., Wahl, T., Santos, V. M., Misra, S. K., & White, K. D. (2022). Assessing the potential for compound storm surge and extreme river discharge events at the catchment scale with statistical models: Sensitivity analysis and recommendations for best practice. *Journal of Hydrologic Engineering*, *27*(3), 04022001. https://doi.org/10.1061/(asce)he.1943-5584.0002154

Jevrejeva, S., Calafat, F. M., De Dominicis, M., Hirschi, J. J.-M., Mecking, J. V., Polton, J. A., et al. (2024). Challenges, advances and opportunities in regional sea level projections: The role of ocean-shelf dynamics. *Earth's Future*, *12*(8), e2024EF004886. https://doi.org/10.1029/2024ef004886

Jonkman, S. N., Maaskant, B., Boyd, E., & Levitan, M. L. (2009). Loss of life caused by the flooding of New Orleans after hurricane Katrina: Analysis of the relationship between flood characteristics and mortality. *Risk Analysis*, *29*(5), 676–698. https://doi.org/10.1111/j.1539-6924.2008.01190.x

Kay, A. (2022). Differences in hydrological impacts using regional climate model and nested convection-permitting model data. *Climatic Change*, *173*(1–2), 11. https://doi.org/10.1007/s10584-022-03405-z

Kay, A. L. (2021). Simulation of river flow in Britain under climate change: Baseline performance and future seasonal changes. *Hydrological Processes*, *35*(4), e14137. https://doi.org/10.1002/hyp.14137

Kay, A. L., Booth, N., Lamb, R., Raven, E., Schaller, N., & Sparrow, S. (2018). Flood event attribution and damage estimation using national-scale grid-based modelling: Winter 2013/2014 in Great Britain. *International Journal of Climatology*, *38*(14), 5205–5219. https://doi.org/10.1002/joc.5721

Kay, A. L., Crooks, S. M., Pall, P., & Stone, D. A. (2011). Attribution of Autumn/Winter 2000 flood risk in England to anthropogenic climate change: A catchment-based study. *Journal of Hydrology*, *406*(1–2), 97–112. https://doi.org/10.1016/j.jhydrol.2011.06.006

Kay, A. L., Watts, G., Wells, S. C., & Allen, S. (2019). The impact of climate change on U.K. river flows: A preliminary comparison of two generations of probabilistic climate projections. *Hydrological Processes*, *34*(4), 1081–1088. https://doi.org/10.1002/hyp.13644

Kendon, E. J., Fosser, G., Murphy, J., Chan, S., Clark, R., & Lowe, J. (2021). *Update of the UKCP18 Local (2.2 km) projections: Results and comparison to observational data*. Met Office. Retrieved from https://www.metoffice.gov.uk/pub/data/weather/uk/ukcp18/science-reports/ukcp18_local_update_report_2021.pdf

Kendon, E. J., Ban, N., Roberts, N. M., Fowler, H. J., Roberts, M. J., Chan, S. C., et al. (2017). Do convection-permitting regional climate models improve projections of future precipitation change? *Bulletin of the American Meteorological Society*, *98*(1), 79–93. https://doi.org/10.1175/BAMS-D-15-0004.1

Kendon, E. J., Prein, A. F., Senior, C. A., & Stirling, A. (2021). Challenges and outlook for convection-permitting climate modelling. *Philosophical Transactions of the Royal Society A: Mathematical, Physical and Engineering Sciences*, *379*(2195), 20190547. https://doi.org/10.1098/rsta.2019.0547

Kendon, E. J., Roberts, N. M., Senior, C. A., & Roberts, M. J. (2012). Realism of rainfall in a very high-resolution regional climate model. *Journal of Climate*, *25*(17), 5791–5806. https://doi.org/10.1175/JCLI-D-11-00562.1

Kendon, E. J., Stratton, R. A., Tucker, S., Marsham, J. H., Berthou, S., Rowell, D. P., & Senior, C. A. (2019). Enhanced future changes in wet and dry extremes over Africa at convection-permitting scale. *Nature Communications*, *10*(1), 1794. https://doi.org/10.1038/s41467-019-09776-9

Kew, S. F., Selten, F. M., Lenderink, G., & Hazeleger, W. (2013). The simultaneous occurrence of surge and discharge extremes for the Rhine delta. *Natural Hazards and Earth System Sciences*, *13*(8), 2017–2029. https://doi.org/10.5194/nhess-13-2017-2013

Khojasteh, D., Glamore, W., Heimhuber, V., & Felder, S. (2021). Sea-level rise impacts on estuarine dynamics: A review. *Science of the Total Environment*, *780*, 146470. https://doi.org/10.1016/j.scitotenv.2021.146470

Kirezci, E., Young, I. R., Ranasinghe, R., Muis, S., Nicholls, R. J., Lincke, D., & Hinkel, J. (2020). Projections of global-scale extreme sea levels and resulting episodic coastal flooding over the 21st century. *Scientific Reports*, *10*(1), 11629. https://doi.org/10.1038/s41598-020-67736-6

Kirkpatrick, J. I. M., & Olbert, A. I. (2020). Modelling the effects of climate change on urban coastal-fluvial flooding. *Journal of Water and Climate Change*, *11*(S1), 270–288. https://doi.org/10.2166/wcc.2020.166

Kulp, S. A., & Strauss, B. H. (2019). New elevation data triple estimates of global vulnerability to sea-level rise and coastal flooding. *Nature Communications*, *10*(1), 4844. https://doi.org/10.1038/s41467-019-12808-z

Kundzewicz, Z. W., & Pińskwar, I. (2022). Are pluvial and fluvial floods on the rise? *Water*, *14*(17), 2612. https://doi.org/10.3390/w14172612

Lane, R. A., & Kay, A. L. (2021). Climate change impact on the magnitude and timing of hydrological extremes across Great Britain. *Frontiers in Water*, *3*, 684982. https://doi.org/10.3389/frwa.2021.684982

Lewis, E., Quinn, N., Blenkinsop, S., Fowler, H. J., Freer, J., Tanguy, M., et al. (2019). *Gridded estimates of hourly areal rainfall for Great Britain (1990-2014) [CEH-GEAR1hr]*. NERC Environmental Information Data Centre. https://doi.org/10.5285/d4ddc781-25f3-423a-bba0-747cc82dc6fa

Lewis, M. J., Palmer, T., Hashemi, R., Robins, P., Saulter, A., Brown, J., et al. (2019). Wave-tide interaction modulates nearshore wave height. *Ocean Dynamics*, *69*(3), 367–384. https://doi.org/10.1007/s10236-018-01245-z

Li, C., Zwiers, F., Zhang, X., Li, G., Sun, Y., & Wehner, M. (2021). Changes in annual extremes of daily temperature and precipitation in CMIP6 models. *Journal of Climate*, *34*(9), 3441–3460. https://doi.org/10.1175/jcli-d-19-1013.1

Lopes, C. L., Sousa, M. C., Ribeiro, A., Pereira, H., Pinheiro, J. P., Vaz, L., & Dias, J. M. (2022). Evaluation of future estuarine floods in a sea-level rise context. *Scientific Reports*, *12*(1), 8083. https://doi.org/10.1038/s41598-022-12122-7

Lowe, J. A., Woodworth, P. L., Knutson, T., McDonald, R. E., McInnes, K. L., Woth, K., et al. (2010). Past and future changes in extreme sea levels and waves. In J. A. Church, P. L. Woodworth, T. Aarup, & W. S. Wilson (Eds.), *Understanding sea-level rise and variability*. Blackwell.

Lyddon, C., Chien, N., Vasilopoulos, G., Ridgill, M., Moradian, S., Olbert, A., et al. (2024). Thresholds for estuarine compound flooding using a combined hydrodynamic–statistical modelling approach. *Natural Hazards and Earth System Sciences*, *24*(3), 973–997. https://doi.org/10.5194/nhess-24-973-2024

Lyddon, C., Robins, P., Lewis, M., Barkwith, A., Vasilopoulos, G., Haigh, I., & Coulthard, T. (2022). Historic spatial patterns of storm-driven compound events in UK estuaries. *Estuaries and Coasts*, *46*(1), 30–56. https://doi.org/10.1007/s12237-022-01115-4

Lyddon, C. E., Brown, J. M., Leonardi, N., & Plater, A. J. (2020). Sensitivity of flood hazard and damage to modelling approaches. *Journal of Marine Science and Engineering*, *8*(9), 724. https://doi.org/10.3390/jmse8090724

Malhi, Y., Franklin, J., Seddon, N., Solan, M., Turner, M. G., Field, C. B., & Knowlton, N. (2020). Climate change and ecosystems: Threats, opportunities and solutions. *Philosophical Transactions of the Royal Society B: Biological Sciences*, *375*(1794), 20190104. https://doi.org/10.1098/rstb.2019.0104

Maraun, D., Widmann, M., Gutiérrez, J. M., Kotlarski, S., Chandler, R. E., Hertig, E., et al. (2015). VALUE: A framework to validate downscaling approaches for climate change studies. *Earth's Future*, *3*(1), 1–14. https://doi.org/10.1002/2014ef000259

Marcos, M., Rohmer, J., Vousdoukas, M. I., Mentaschi, L., Le Cozannet, G., & Amores, A. (2019). Increased extreme coastal water levels due to the combined action of storm surges and wind waves. *Geophysical Research Letters*, *46*(8), 4356–4364. https://doi.org/10.1029/2019gl082599

Marsooli, R., Lin, N., Emanuel, K., & Feng, K. (2019). Climate change exacerbates hurricane flood hazards along US Atlantic and Gulf Coasts in spatially varying patterns. *Nature Communications*, *10*(1), 3785. https://doi.org/10.1038/s41467-019-11755-z

Meli, M., Camargo, C. M. L., Olivieri, M., Slangen, A. B. A., & Romagnoli, C. (2023). Sea-level trend variability in the Mediterranean during the 1993–2019 period. *Frontiers in Marine Science*, *10*, 1150488. https://doi.org/10.3389/fmars.2023.1150488

Meli, M., Olivieri, M., & Romagnoli, C. (2020). Sea-level change along the Emilia-Romagna Coast from tide gauge and satellite altimetry. *Remote Sensing*, *13*(1), 97. https://doi.org/10.3390/rs13010097

Menéndez, M., & Woodworth, P. L. (2010). Changes in extreme high water levels based on a quasi-global tide-gauge data set. *Journal of Geophysical Research*. https://doi.org/10.1029/2009jc005997

Merz, B., Blöschl, G., Vorogushyn, S., Dottori, F., Aerts, J. C. J. H., Bates, P., et al. (2021). Causes, impacts and patterns of disastrous river floods. *Nature Reviews Earth & Environment*, *2*(9), 592–609. https://doi.org/10.1038/s43017-021-00195-3

Met Office Hadley Centre. (2018). UKCP18 21st century time-mean sea level projections around the UK for 2007-2100 [Dataset]. *Centre for Environmental Data Analysis*. Retrieved from https://catalogue.ceda.ac.uk/uuid/0f8d27b1192f41088cd6983e98faa46e/

Moftakhari, H., Schubert, J. E., AghaKouchak, A., Matthew, R. A., & Sanders, B. F. (2019). Linking statistical and hydrodynamic modeling for compound flood hazard assessment in tidal channels and estuaries. *Advances in Water Resources*, *128*, 28–38. https://doi.org/10.1016/j.advwatres.2019.04.009

Muis, S., Apecechea, M. I., Dullaart, J., de Lima Rego, J., Madsen, K. S., Su, J., et al. (2020). A high-resolution global dataset of extreme sea levels, tides, and storm surges, including future projections. *Frontiers in Marine Science*, *7*, 263. https://doi.org/10.3389/fmars.2020.00263

Muis, S., Verlaan, M., Winsemius, H. C., Aerts, J. C. J. H., & Ward, P. J. (2016). A global reanalysis of storm surges and extreme sea levels. *Nature Communications*, *7*(1), 11969. https://doi.org/10.1038/ncomms11969

Murphy, J. M., Harris, G. R., Sexton, D. M. H., Kendon, E. J., Bett, P. E., Brown, S. J., et al. (2018). *UKCP18 land projections: Science report*. Met Office Hadley Centre. Retrieved from https://www.metoffice.gov.uk/pub/data/weather/uk/ukcp18/science-reports/UKCP18-Overview-report.pdf

Nash, J. E., & Sutcliffe, J. V. (1970). River flow forecasting through conceptual models part I—A discussion of principles. *Journal of Hydrology*, *10*(3), 282–290. https://doi.org/10.1016/0022-1694(70)90255-6

National Tidal and Sea Level Facility (NTSLF). (2022). Dyfi at Dyfi bridge [Dataset]. Retrieved from https://nrfa.ceh.ac.uk/data/station/info/64001

Natural Resource Wales. (2020). Flood defence structures [Dataset]. Retrieved from https://datamap.gov.wales/layergroups/geonode:nrw_flood_defence_structures

Neumann, B., Vafeidis, A. T., Zimmermann, J., & Nicholls, R. J. (2015). Future coastal population growth and exposure to sea-level rise and coastal flooding - A global assessment. *PLoS One*, *10*(3), e0118571. https://doi.org/10.1371/journal.pone.0118571

Nicholls, R. J., Lincke, D., Hinkel, J., Brown, S., Vafeidis, A. T., Meyssignac, B., et al. (2021). A global analysis of subsidence, relative sea-level change and coastal flood exposure. *Nature Climate Change*, *11*(4), 338–342. https://doi.org/10.1038/s41558-021-00993-z

Orr, H. G., Ekström, M., Charlton, M. B., Peat, K. L., & Fowler, H. J. (2021). Using high-resolution climate change information in water management: A decision-makers' perspective. *Philosophical Transactions of the Royal Society A: Mathematical, Physical and Engineering Sciences*, *379*(2195), 20200219. https://doi.org/10.1098/rsta.2020.0219

Palmer, M., Howard, T., Tinker, J., Lowe, J., Bricheno, L., Calvert, D., et al. (2018). *UKCP18 marine report*. Met Office Hadley Centre.

Paprotny, D., Sebastian, A., Morales-Nápoles, O., & Jonkman, S. N. (2018). Trends in flood losses in Europe over the past 150 years. *Nature Communications*, *9*(1), 1985. https://doi.org/10.1038/s41467-018-04253-1

Paprotny, D., Vousdoukas, M. I., Morales-Nápoles, O., Jonkman, S. N., & Feyen, L. (2020). Pan-European hydrodynamic models and their ability to identify compound floods. *Natural Hazards*, *101*(3), 933–957. https://doi.org/10.1007/s11069-020-03902-3

Paschalis, A., Molnar, P., Fatichi, S., & Burlando, P. (2014). On temporal stochastic modeling of precipitation, nesting models across scales. *Advances in Water Resources*, *63*, 152–166. https://doi.org/10.1016/j.advwatres.2013.11.006

Pawlowicz, R., Beardsley, B., & Lentz, S. (2002). Classical tidal harmonic analysis including error estimates in MATLAB using T_TIDE. *Computers & Geosciences*, *28*(8), 929–937. https://doi.org/10.1016/s0098-3004(02)00013-4

Peleg, N., Skinner, C., Fatichi, S., & Molnar, P. (2020). Temperature effects on the spatial structure of heavy rainfall modify catchment hydro-morphological response. *Earth Surface Dynamics*, *8*(1), 17–36. https://doi.org/10.5194/esurf-8-17-2020

Ponte, R. M., Carson, M., Cirano, M., Domingues, C. M., Jevrejeva, S., Marcos, M., et al. (2019). Towards comprehensive observing and modeling systems for monitoring and predicting regional to coastal sea level. *Frontiers in Marine Science*, *6*, 437. https://doi.org/10.3389/fmars.2019.00437

Prampolini, M., Savini, A., Foglini, F., & Soldati, M. (2020). Seven good reasons for integrating terrestrial and marine spatial datasets in changing environments. *Water*, *12*(8), 2221. https://doi.org/10.3390/w12082221

Prein, A. F., Langhans, W., Fosser, G., Ferrone, A., Ban, N., Goergen, K., et al. (2015). A review on regional convection-permitting climate modeling: Demonstrations, prospects, and challenges. *Reviews of Geophysics*, *53*(2), 323–361. https://doi.org/10.1002/2014rg000475

Pugh, D. T., & Maul, G. A. (1999). Coastal sea level, prediction for climate change. In C. N. K. Mooers (Ed.), *Coastal and estuarine studies* (Vol. 56, pp. 377–404). AGU. https://doi.org/10.1029/ce056p0377

Ranasinghe, R., Ruane, A. C., Vautard, R., Arnell, N., Coppola, E., Cruz, F. A., et al. (2021). Climate change information for regional impact and for risk assessment. In *Climate change 2021: The physical science basis. Contribution of working group 1 to the sixth assessment report of the intergovernmental panel on climate change* (pp. 1767–1926). Cambridge University Press. https://doi.org/10.1017/9781009157896.014

Redfern, T. W., Macdonald, N., Kjeldsen, T. R., Miller, J. D., & Reynard, N. (2016). Current understanding of hydrological processes on common urban surfaces. *Progress in Physical Geography: Earth and Environment*, *40*(5), 699–713. https://doi.org/10.1177/0309133316652819

Reimann, L., Vafeidis, A. T., & Honsel, L. E. (2023). Population development as a driver of coastal risk: Current trends and future pathways. *Cambridge Prisms: Coastal Futures*, *1*, e14. https://doi.org/10.1017/cft.2023.3

Robins, P. E., & Davies, A. G. (2010). Morphological controls in sandy estuaries: The influence of tidal flats and bathymetry on sediment transport. *Ocean Dynamics*, *60*(3), 503–517. https://doi.org/10.1007/s10236-010-0268-4

Robins, P. E., Lewis, M. J., Elnahrawi, M., Lyddon, C., Dickson, N., & Coulthard, T. J. (2021). Compound flooding: Dependence at sub-daily scales between extreme storm surge and fluvial flow. *Frontiers in Built Environment*, *7*, 727294. https://doi.org/10.3389/fbuil.2021.727294

Robins, P. E., Lewis, M. J., Freer, J., Cooper, D. M., Skinner, C. J., & Coulthard, T. J. (2018). Improving estuary models by reducing uncertainties associated with river flows. *Estuarine, Coastal and Shelf Science*, *207*, 63–73. https://doi.org/10.1016/j.ecss.2018.02.015

Robins, P. E., Skov, M. W., Lewis, M. J., Giménez, L., Davies, A. G., Malham, S. K., et al. (2016). Impact of climate change on UK estuaries: A review of past trends and potential projections. *Estuarine, Coastal and Shelf Science*, *169*, 119–135. https://doi.org/10.1016/j.ecss.2015.12.016

Rudd, A. C., Kay, A. L., Wells, S. C., Aldridge, T., Cole, S. J., Kendon, E. J., & Stewart, E. J. (2019). Investigating potential future changes in surface water flooding hazard and impact. *Hydrological Processes*, *34*(1), 139–149. https://doi.org/10.1002/hyp.13572

Schaller, N., Sillmann, J., Müller, M., Haarsma, R., Hazeleger, W., Hegdahl, T. J., et al. (2020). The role of spatial and temporal model resolution in a flood event storyline approach in western Norway. *Weather and Climate Extremes*, *29*, 100259. https://doi.org/10.1016/j.wace.2020.100259

Seenath, A. (2018). Effects of DEM resolution on modeling coastal flood vulnerability. *Marine Geodesy*, *41*(6), 581–604. https://doi.org/10.1080/01490419.2018.1504838

Seneviratne, S. I., Zhang, X., Adnan, M., Badi, W., Dereczynski, C., Luca, A. D., et al. (2021). Weather and climate extreme events in a changing climate. In V. P. Masson-Delmotte, A. Zhai, S. L. Pirani, & C. Connors (Eds.), *Climate change 2021: The physical science basis: Working group I contribution to the sixth assessment report of the intergovernmental panel on climate change* (pp. 1513–1766). Cambridge University Press.

Sexton, D. M. H., McSweeney, C. F., Rostron, J. W., Yamazaki, K., Booth, B. B. B., Murphy, J. M., et al. (2021). A perturbed parameter ensemble of HadGEM3-GC3.05 coupled model projections: Part 1: Selecting the parameter combinations. *Climate Dynamics*, *56*(11–12), 3395–3436. https://doi.org/10.1007/s00382-021-05709-9

Shi, Z. (1993). Recent saltmarsh accretion and sea level fluctuations in the Dyfi Estuary, central Cardigan Bay, Wales, UK. *Geo-Marine Letters*, *13*(3), 182–188. https://doi.org/10.1007/bf01593192

Steinhausen, M., Paprotny, D., Dottori, F., Sairam, N., Mentaschi, L., Alfieri, L., et al. (2022). Drivers of future fluvial flood risk change for residential buildings in Europe. *Global Environmental Change*, *76*, 102559. https://doi.org/10.1016/j.gloenvcha.2022.102559

Svensson, C., & Jones, D. A. (2002). Dependence between extreme sea surge, river flow and precipitation in eastern Britain. *International Journal of Climatology*, *22*(10), 1149–1168. https://doi.org/10.1002/joc.794

Svensson, C., & Jones, D. A. (2004). Dependence between sea surge, river flow and precipitation in south and west Britain. *Hydrology and Earth System Sciences*, *8*(5), 973–992. https://doi.org/10.5194/hess-8-973-2004

Tabari, H. (2020). Climate change impact on flood and extreme precipitation increases with water availability. *Scientific Reports*, *10*(1), 13768. https://doi.org/10.1038/s41598-020-70816-2

Tanguy, M., Prudhomme, C., Smith, K., & Hannaford, J. (2018). Historical gridded reconstruction of potential evapotranspiration for the UK. *Earth System Science Data*, *10*(2), 951–968. https://doi.org/10.5194/essd-10-951-2018

Taylor, K. E., Stouffer, R. J., & Meehl, G. A. (2012). An overview of CMIP5 and the experiment design. *Bulletin of the American Meteorological Society*, *93*(4), 485–498. https://doi.org/10.1175/bams-d-11-00094.1

Tebaldi, C., Ranasinghe, R., Vousdoukas, M., Rasmussen, D. J., Vega-Westhoff, B., Kirezci, E., et al. (2021). Extreme sea levels at different global warming levels. *Nature Climate Change*, *11*(9), 746–751. https://doi.org/10.1038/s41558-021-01127-1

Tinker, J. (2023). Physical marine climate projections for the North West European Shelf Seas: NWSPPE [Dataset]. *NERC EDS Centre for Environmental Data Analysis*. https://doi.org/10.5285/edf66239c70c426e9e9f19da1ac8ba87

Tinker, J., Palmer, M. D., Copsey, D., Howard, T., Lowe, J. A., & Hermans, T. H. J. (2020). Dynamical downscaling of unforced interannual sea-level variability in the North-West European shelf seas. *Climate Dynamics*, *55*(7–8), 2207–2236. https://doi.org/10.1007/s00382-020-05378-0

Tinker, J., Palmer, M. D., Harrison, B. J., O'Dea, E., Sexton, D. M. H., Yamazaki, K., & Rostron, J. W. (2024). Twenty-first century marine climate projections for the NW European shelf seas based on a perturbed parameter ensemble. *Ocean Science*, *20*(3), 835–885. https://doi.org/10.5194/os-20-835-2024

Toimil, A., Losada, I. J., Nicholls, R. J., Dalrymple, R. A., & Stive, M. J. F. (2020). Addressing the challenges of climate change risks and adaptation in coastal areas: A review. *Coastal Engineering*, *156*, 103611. https://doi.org/10.1016/j.coastaleng.2019.103611

Tucker, S. O., Kendon, E. J., Bellouin, N., Buonomo, E., Johnson, B., & Murphy, J. M. (2021). Evaluation of a new 12 km regional perturbed parameter ensemble over Europe. *Climate Dynamics*, *58*(3–4), 879–903. https://doi.org/10.1007/s00382-021-05941-3

Vitousek, S., Barnard, P. L., Fletcher, C. H., Frazer, N., Erikson, L., & Storlazzi, C. D. (2017). Doubling of coastal flooding frequency within decades due to sea-level rise. *Scientific Reports*, *7*(1), 1399. https://doi.org/10.1038/s41598-017-01362-7

Vousdoukas, M. I., Mentaschi, L., Voukouvalas, E., Verlaan, M., Jevrejeva, S., Jackson, L. P., & Feyen, L. (2018). Global probabilistic projections of extreme sea levels show intensification of coastal flood hazard. *Nature Communications*, *9*(1), 2360. https://doi.org/10.1038/s41467-018-04692-w

Wahl, T., Jain, S., Bender, J., Meyers, S. D., & Luther, M. E. (2015). Increasing risk of compound flooding from storm surge and rainfall for major US cities. *Nature Climate Change*, *5*(12), 1093–1097. https://doi.org/10.1038/nclimate2736

Wang, Y., Zhang, X., Zhao, K., & Singh, D. (2024). Streamflow in the United States: Characteristics, trends, regime shifts, and extremes. *Scientific Data*, *11*(1), 788. https://doi.org/10.1038/s41597-024-03618-0

Ward, P. J., Couasnon, A., Eilander, D., Haigh, I. D., Hendry, A., Muis, S., et al. (2018). Dependence between high sea-level and high river discharge increases flood hazard in global deltas and estuaries. *Environmental Research Letters*, *13*(8), 084012. https://doi.org/10.1088/1748-9326/aad400

Watson, C. S., White, N. J., Church, J. A., King, M. A., Burgette, R. J., & Legresy, B. (2015). Unabated global mean sea-level rise over the satellite altimeter era. *Nature Climate Change*, *5*(6), 565–568. https://doi.org/10.1038/nclimate2635

Weisscher, S. A. H., Adema, P. H., Rossius, J., & Kleinhans, M. G. (2023). The effect of sea-level rise on estuary filling in scaled landscape experiments. *The Depositional Record*, *9*(2), 363–379. https://doi.org/10.1002/dep2.233

Westra, S., Alexander, L. V., & Zwiers, F. W. (2013). Global increasing trends in annual maximum daily precipitation. *Journal of Climate*, *26*(11), 3904–3918. https://doi.org/10.1175/jcli-d-12-00502.1

Williams, K. D., Copsey, D., Blockley, E. W., Bodas-Salcedo, A., Calvert, D., Comer, R., et al. (2018). The Met Office Global Coupled Model 3.0 and 3.1 (GC3.0 and GC3.1) configurations. *Journal of Advances in Modeling Earth Systems*, *10*(2), 357–380. https://doi.org/10.1002/2017ms001115

Wing, O. E. J., Bates, P. D., Sampson, C. C., Smith, A. M., Johnson, K. A., & Erickson, T. A. (2017). Validation of a 30 m resolution flood hazard model of the conterminous United States. *Water Resources Research*, *53*(9), 7968–7986. https://doi.org/10.1002/2017wr020917

Woth, K., Weisse, R., & von Storch, H. (2005). Climate change and North Sea storm surge extremes: An ensemble study of storm surge extremes expected in a changed climate projected by four different regional climate models. *Ocean Dynamics*, *56*(1), 3–15. https://doi.org/10.1007/s10236-005-0024-3

Yin, J., Gentine, P., Zhou, S., Sullivan, S. C., Wang, R., Zhang, Y., & Guo, S. (2018). Large increase in global storm runoff extremes driven by climate and anthropogenic changes. *Nature Communications*, *9*(1), 4389. https://doi.org/10.1038/s41467-018-06765-2

Zellou, B., & Rahali, H. (2019). Assessment of the joint impact of extreme rainfall and storm surge on the risk of flooding in a coastal area. *Journal of Hydrology*, *569*, 647–665. https://doi.org/10.1016/j.jhydrol.2018.12.028

Zhang, F., Lin, B., & Sun, J. (2019). Current reversals in a large tidal river. *Estuarine, Coastal and Shelf Science*, *223*, 74–84. https://doi.org/10.1016/j.ecss.2019.04.017

Zscheischler, J., & Seneviratne, S. I. (2017). Dependence of drivers affects risks associated with compound events. *Science Advances*, *3*(6), e1700263. https://doi.org/10.1126/sciadv.1700263